PAPER • OPEN ACCESS

Observation of alpha-particles in recent D–T experiments on JET

OPEN ACCESS
IOP Publishing | International Atomic Energy Agency
Nuclear Fusion
Nucl. Fusion **64** (2024) 086059 (20pp)
https://doi.org/10.1088/1741-4326/ad5c81

Observation of alpha-particles in recent D–T experiments on JET

V.G. Kiptily[1,*], C.D. Challis[1], R. Dumont[2], M. Fitzgerald[1], J. Garcia[2], L. Garzotti[1], Z. Ghani[1], J. Hobirk[3], P. Jacquet[1], A. Kappatou[3], D. Keeling[1], Ye. Kazakov[4], P. Mantica[5], M.J. Mantsinen[6,7], S.E. Sharapov[1], E.R. Solano[8], D. Van Eester[4], P.J. Bonofiglo[9], T. Craciunescu[10], A. Dal Molin[11], J. Eriksson[12], V. Goloborodko[13], M.V. Iliasova[14], E.M. Khilkevitch[14], D. King[1], I. Lengar[15], M. Nocente[16], S. Menmuir[1], M. Podestà[9], M. Poradzinski[1], D. Rigamonti[11], J. Rivero-Rodriguez[1,17], Z. Stancar[1,15], A.E. Shevelev[14], P. Siren[1], H. Sun[1], D.M. Taylor[1], M. Tardocchi[16], P. Beaumont[1], F. Belli[18], F.E. Cecil[19], R. Coelho[20], M. Curuia[21], M. Garcia-Munoz[16], E. Joffrin[2], C. Lowry[1], M. Lennholm[1], E. Lerche[4], C.F. Maggi[1], J. Mailloux[1], D. Marocco[18], M. Maslov[1], C. Perez Von Thun[22], F. Rimini[1], V. Zoita[10] and JET Contributors[a]

[1] United Kingdom Atomic Energy Authority, Abingdon, Oxon OX14 3DB, United Kingdom of Great Britain and Northern Ireland
[2] CEA, IRFM, F-13108 Saint-Paul-Lez-Durance, France
[3] Max-Planck-Institut für Plasmaphysik, Boltzmannstr. 2, 85748 Garching, Germany
[4] LPP-ERM/KMS, Association EUROFUSION-Belgian State, TEC partner, Brussels, Belgium
[5] Istituto per la Scienza e Tecnologia Dei Plasmi, Consiglio Nazionale Delle Ricerche, Milano, Italy
[6] Barcelona Supercomputing Centtre, Barcelona, Spain
[7] ICREA, Pg. LiuisCompanys23, 08010 Barcelona, Spain
[8] Laboratorio Nacional de Fusión, CIEMAT, Madrid, Spain
[9] Princeton Plasma Physics Laboratory, Princeton NJ 08543, NJ, United States of America
[10] National Institute for Laser, Plasma and Radiation Physics, Bucharest, Romania
[11] Institute for Plasma Science and Technology, National Research Council, Milan, Italy
[12] Department of Physics and Astronomy, Uppsala University, BOX 516 Uppsala, Sweden
[13] Kyiv Institute for Nuclear Research, ProspektNauky47, Kyiv 03680, Ukraine
[14] Ioffe Physico-Technical Institute, 26 Politekhnicheskaya, St Petersburg 194021, Russian Federation
[15] Jožef Stefan Institute, Jamova 39, SI-1000 Ljubljana, Slovenia
[16] Dipartimento di Fisica, Università di Milano-Bicocca, Milan, Italy
[17] FAMN Department, Faculty of Physics, University of Seville, 41012 Seville, Spain
[18] Unità Tecnica Fusione -ENEA C. R. Frascati, via E. Fermi 45, 00044 Frascati (Roma), Italy
[19] Colorado School of Mines, Golden, CO 80401, United States of America
[20] Instituto de Plasmas e Fusao Nuclear, Instituto Superior Técnico, Universidade de Lisboa, 1049-001 Lisboa, Portugal
[21] National Institute for Cryogenics and Isotopic Technology, Bucharest, Romania
[22] Institute of Plasma Physics and Laser Microfusion (IPPLM), Hery 23, 01-497 Warsaw, Poland

[a] See Maggi *et al* 2024 (https://doi.org/10.1088/1741-4326/ad3e16) for JET Contributors.
[*] Author to whom any correspondence should be addressed.

E-mail: Vasili.Kiptily@ukaea.uk

Received 14 February 2024, revised 14 June 2024
Accepted for publication 27 June 2024
Published 11 July 2024

Abstract

The fusion reaction between deuterium and tritium, $D(T,n)^4He$ is the main source of energy in future thermonuclear reactors. Alpha-particles (^4He-ions) born with an average energy of 3.5 MeV transferring energy to the thermal plasma during their slowing down, should provide the self-sustained *D–T* plasma burn. The adequate confinement of α-particles is essential to provide efficient heating of the bulk plasma and steady burning of a reactor plasma. That is why the fusion-born α-particle studies have been a priority task in the second *D–T* experiments (DTE2) on the Joint European Torus (JET) to understand the main mechanisms of their slowing down, redistribution and losses and to develop optimal plasma scenarios. JET with *Be*-wall and *W*-divertor, enhanced auxiliary heating systems and improved energetic-particle diagnostic capabilities, producing significant population of α-particles, provided the possibility for comprehensive studying of the α-particle behaviour. Selected results of the confined and lost α-particle measurements, evidence of α-particle self-heating and assessments of the fusion performance are presented in this paper giving an opportunity for further modelling and extrapolation to the International Thermonuclear Experimental Reactor and burning plasma reactors.

Keywords: JET, DT-plasmas, fusion, alpha-particles

(Some figures may appear in colour only in the online journal)

1. Introduction

The fusion reaction between deuterium (D) and tritium (T), $D(T,n)^4He$ is the main source of energy ($\gtrsim$17.6 MeV per fusion) in future thermonuclear reactors. The charged fusion product of this reaction, ^4He-ions (α-particles), born with energy of $\approx$3.5 MeV, should provide the self-sustained *D–T* plasma burn, transferring energy to the thermal plasma during their slowing down. An adequate confinement of α-particles is essential to provide efficient heating of the bulk plasma and steady burning of a reactor plasma. That is why the fusion-born α-particle studies were a priority task for DTE2 [1], the second *D–T* experiments on Joint European Torus (JET). The goal is to understand the main mechanisms of their slowing down, redistribution and losses developing optimal, effective plasma scenarios for International Thermonuclear Experimental Reactor (ITER) and future fusion reactors with magnetic confinement. JET, with beryllium wall, tungsten divertor and enhanced auxiliary heating systems, produced significant population of α-particles in *D-T* plasmas and provided a great opportunity to study the α-particle behaviour, giving a stepladder approach for modelling and extrapolating to ITER. Results from a number of JET plasma pulses are selected and discussed in the present work in which the above-mentioned phenomena are most clearly observed. In addition, the topic of plasma self-heating [2] is revisited to expand the discussion to additional relevant α-particle effects.

The full-scale *D–T* experiments on the tokamak fusion test reactor (TFTR) [3] and JET [4] in 1997 (DTE1) have shown that direct measurements of alphas are very difficult. Alpha-particle studies require a significant development of dedicated diagnostics for both confined and lost α-particles. To make such measurements be possible, JET being a test-bed for ITER, was equipped with a dedicated set of fast α-particle diagnostics for operation at the high neutron and γ-ray fluxes in the *D–T* experiments. Neutron and γ-ray spectrometers and 2D neutron camera were fully upgraded. The fast-ion loss detector with energy and pitch-angle resolution (FILD) and a set of lost α-particle collectors with poloidal, radial and energy resolution (Faraday Cups) were installed. The detailed description of the α-particle diagnostics can be found in the next section.

Selected results of α-particle studies in DTE2 are presented in this paper. Direct evidence of the α-particle self-heating and assessments of the fusion performance in the afterglow plasma are given in section 3. Confinement of fast α-particles produced in the *D–T* fusion plasma is of crucial importance for future reactors. Measurements of the first ever attempt of confined α-particle diagnosing are discussed in section 4. Plasma instabilities may lead to significant α-particle losses and the loss of plasma heating that is not acceptable for an efficient fusion plant as it can cause problems getting to the burning state and damage to the first wall. In section 5 we present the α-particle loss effects related to magneto-hydro-dynamic (MHD) activities in *D–T* plasmas. Fusion γ-rays, 17 MeV γ-rays due to the $D(T,\gamma)^5He$ reaction and 20 MeV γ-rays of the $T(H,\gamma)^4He$ reaction, were measured in *D–T* and tritium plasmas with the *H*-minority ICRF heating. These important results obtained for the first time are shown in section 6. Finally, a summary and conclusions of the paper are presented in the last section.

2. Alpha-particle diagnostics

In the preparation of DTE2, dedicated α-particle diagnostics were developed, so JET was equipped with a unique set of diagnostics for operation at the high neutron and γ-ray fluxes in *D–T* experiments.

2.1. Alpha-particle source profile measurements

The JET plasma heating, with beam injection of the energetic deuterium and tritium neutrals (NBI) and with waves in the ion-cyclotron range of frequencies (ICRF), leads to the fact that in some plasma scenarios the beam-target fusion reaction rate could be substantial, so the energetic ion power deposition and, hence, the α-particle source profile measurements are rather important for dedicated studies of the confined and lost α-particles. An exciting evolution of the *D–T* α-particle source has been measured with JET 2D neutron camera during *D*-NBI heating of the *D*-plasma with *T*-puff [5]. Also, plasma instabilities, for example sawtooth oscillations, interacting with *D*-beam ions accelerated by ICRF are causing a dramatic *D-*^{3}*He* α-particle source profile change [6].

The JET neutron profile monitor [7, 8] consists of 2 fan-shaped array cameras with 19 collimated viewing channels (9 vertical and 10 horizontal), which has 2 independent rotatable collimators with 10- and 21 mm apertures each. The plasma coverage is acceptable for tomography reconstructions. Two sets of neutron detectors, NE213 liquid scintillators used for 2.5 MeV *D–D* and 14 MeV *D–T* neutrons and BC418 plastic scintillators for *D–T* neutrons detection, are available. Both sets are equipped with individual digital data acquisition systems that allow measurements in DTE2. Also, in front of the neutron detectors γ-ray spectrometers can be setup, which are placed on the movable rail. The 2D γ-ray camera that already used for tomographic reconstruction of the HXR emission due to runaways and γ-rays produced by fast ions [9], in particular 17 MeV γ-rays related to the *D-*^{3}*He* fusion, can also provide the α-particle source profile [10].

2.2. Gamma-ray spectrometers

Gamma-ray diagnosis is one of the important techniques used on JET for studying confined fast ions [11]. Four high-performance γ-ray spectrometers were installed on JET. Three of them, $LaBr_3(Ce)$ scintillators and Hp*Ge*-detector (a high purity *Ge*-detector is placed on a remotely controlled slider sharing the same line-of-sight with the scintillator) are viewing the plasma centre vertically through 2 m collimators equipped with neutron attenuators. The fourth one, $LaBr_3(Ce)$ scintillator with a tangential field-of-view with an improved neutron attenuation [12, 13]. The $LaBr_3(Ce)$ scintillator has a short decay time of $\sim$20 ns and high photo-yield. The $LaBr_3(Ce)$ spectrometers have the counting rate limit beyond 1 MHz, and at the same time a high energy resolution [14]. The γ-ray spectra are continuously recorded in all JET discharges over the energy range 1–30 MeV.

The feasibility of γ-ray measurements in *D–T* discharges depends on the efficiency of the neutron suppression. The best neutron attenuator is ^6LiH, however, a natural lithium composition, *LiH*, is used on JET [12]. It is compact, effective and nearly transparent to MeV γ-rays; it does not generate interfering γ-rays in the high-energy range, therefore the *LiH* neutron attenuator substantially reduced the γ-ray background.

2.3. Confined α-particle diagnostics

On JET, with beryllium as a main impurity in the plasma, the confined α-particle diagnosing is based on detection of γ-rays due to the nuclear reaction $^9Be(\alpha,n\gamma)^{12}C$ between confined α-particles and the beryllium [15] that has a specific reaction cross-section. The excitation of the first two levels in the final nucleus ^{12}C has a resonance pattern, so emission of the 4.44 MeV γ-rays is evidence for the confined alphas with energies that exceed 1.7 MeV. Furthermore, detection of the 3.21 MeV γ-rays indicates that α-particles with energies more than 4 MeV exist in the plasma. The γ-radiation due to this reaction has been measured by scintillator spectrometers in JET experiments with the 3rd harmonic ICRF accelerating of ^4He-beam ions in a ^4He-plasma [16, 17] and in deuterium plasmas with short tritium-NBI blips causing the α-particles flash and their following slowing down [18]. The high resolution *HpGe*-detector has allowed the α-particle diagnosing with the Doppler shape analysis (DSA) of the 4.44 MeV γ-ray line broadened in the nuclear reaction $^9Be(\alpha,n\gamma)^{12}C$. The DSA technique has been tested in the 3rd harmonic acceleration of a ^4He-beam ions and ^3He-minority ICRF heating experiments [19–21].

2.4. Fast ion loss detectors (FILDs)

Two devices have been installed in the JET vacuum vessel near the plasma boundary to measure the loss of energetic ions and fusion products, in particular α-particles during the *D–T* experiments. The first detector is an array of multichannel thin-foil charge collectors (Faraday Cups) with poloidal, radial and energy resolution [22, 23]. The second one is a well collimated scintillator probe (SP) providing gyro-radius (G-R) (energy) and pitch-angle (P-A) resolution, which is optically connected to a charge-coupled device (CCD) and array of 16 photomultipliers (PMT) equipped with 2 MHz digitisers [24, 25]. The high-frequency digitisers have allowed comparison of both fusion-product losses and Mirnov coil spectrograms to identify the resonant MHD modes [26]. These diagnostics provided important α-particle measurements in DTE2.

3. Alpha-particle heating and fusion performance

In high-power experiments in TFTR [27, 28] it was found that the energy stored in the electron and ions increased by $\sim$20% in the $n_D \approx n_T$ plasma compared to similar pure deuterium plasmas. Eliminating the isotopic and MHD effects, it was stated that the increase took place both due to improved confinement associated with the use of tritium, and probably heating of electrons by *D–T* α-particles. Later, in DTE1 experiments with the fuel mixture scan, separating the effects

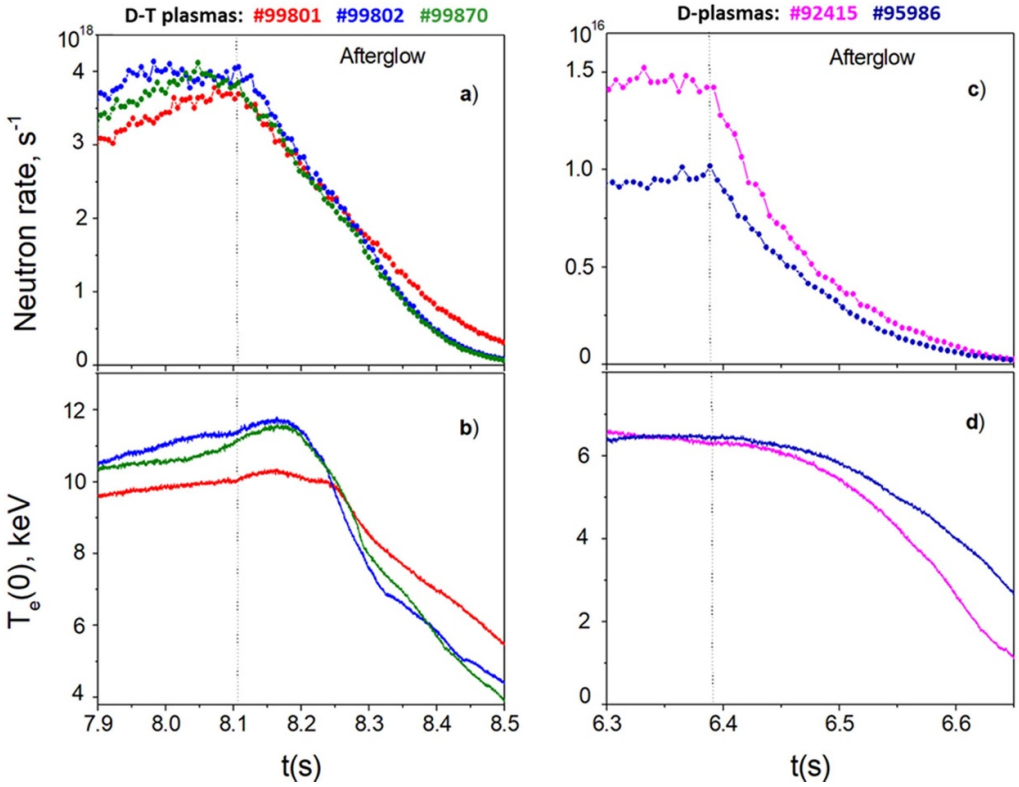

Figure 1. Waveforms of JET discharges with NBI afterglow: (*a*) and (*b*)—the D–T pulses; (*c*) and (*d*)—the deuterium pulses (the time axes were adjusted in time to align NBI cuts). The panels show waveforms of central electron temperatures, $T_e(0)$, and measured neutron rates; the dash line is marking the start of the NBI afterglow period.

of improved confinement and α-particle heating [29], the α-particle heating effects were seen in the electron temperature and energy content.

In the recent DTE2 experiments the direct α-particle self-heating was identified in high-performance plasma discharges with power modulation of *D*- and *T*-NBI but without ICRF heating [2]. It was observed that in the NBI afterglow period the total neutron rate (substantially *D–T* neutrons) is decreasing while the plasma core electron temperature, $T_e(0)$, measured by the electron cyclotron emission diagnostics, is still increasing for a short period. This evolution of the temperature is in a contrast to the reference high-performance deuterium discharges, in which both T_e and *D–D* neutron rate are decreasing during the NBI afterglow. The α-particle self-heating effect was observed in both the so-called hybrid scenario [30] discharges as well as in discharges with an internal transport barrier (ITB) [31]. A comparison of some *D–T* and deuterium discharges with NBI cuts are presented in figure 1.

A detailed analysis of the observed effect has been performed for the *D–T* discharge #99801 fuelled with approximately equal densities of deuterium and tritium, $n_D \approx n_T$, and the reference a deuterium discharge [2]. Both discharges were delivered at the toroidal magnetic field $B_0 = 3.45$ T on the magnetic axis, plasma current is $I_p = 2.3$ MA and the electron density $n_{e0} \approx 4.3 \times 10^{19}\,\mathrm{m}^{-3}$, a central line averaged density measured by far infrared diagnostic system (FIR interferometry). The neutral *D*- and *T*-beams with energies $E_{NBI} \approx 105-115$ keV were injected to heat the fuel ions. A maximum NBI heating power of $P_{NBI} \approx 26$ MW was injected by radial and tangential neutral beams; the NBI afterglow period was from $t = 8.105$ s to $t = 8.5$s as expected that is sufficient for thermalisation.

At the peak performance of the *D–T* discharge just before the NBI cut, the core electron temperature gain is about 30% at same heating conditions with deuterium discharge. Note, that in contrast to the reference deuterium discharge, the difference between the ion and electron temperatures is growing during NBI heating.

In the beginning of the afterglow period, the *D–T* core electron temperature has a trend with $\mathrm{d}T_e/\mathrm{d}t \geqslant 0$ for a while, reaching $T_e(0) \approx 10.3$ keV, and it is slightly decreasing to $\sim$10 keV then. Thus, the core electron temperature of the *D–T* plasma remained in the range 10–10.3 keV without any auxiliary heating. It is not the case in the deuterium pulse afterglow.

Note, the slowing down of the 3.5 MeV α-particles is predominantly due to electron friction since their energy $E_\alpha \gg E_{crit} \approx 0.38$ MeV (according to [32], at the critical energy of ions, E_{crit}, the rate of loss of energy to the plasma electrons and to the ions equal). At the same time, thermalisation of NBI ions occurs mainly due to interaction with fuel ions because of $E_{T\text{-}NBI} < E_{crit} \approx 0.31$ MeV and $E_{D\text{-}NBI} < E_{crit} \approx 0.21$ MeV. Hence, the *D*- and *T*-beam ions are mostly heating the plasma fuel ions, merely 3.5 MeV *D–T* α-particles could heat electrons. The ion-electron slowing down time of 3.5 MeV alphas, is $\sim$910 ms [33]. As a result

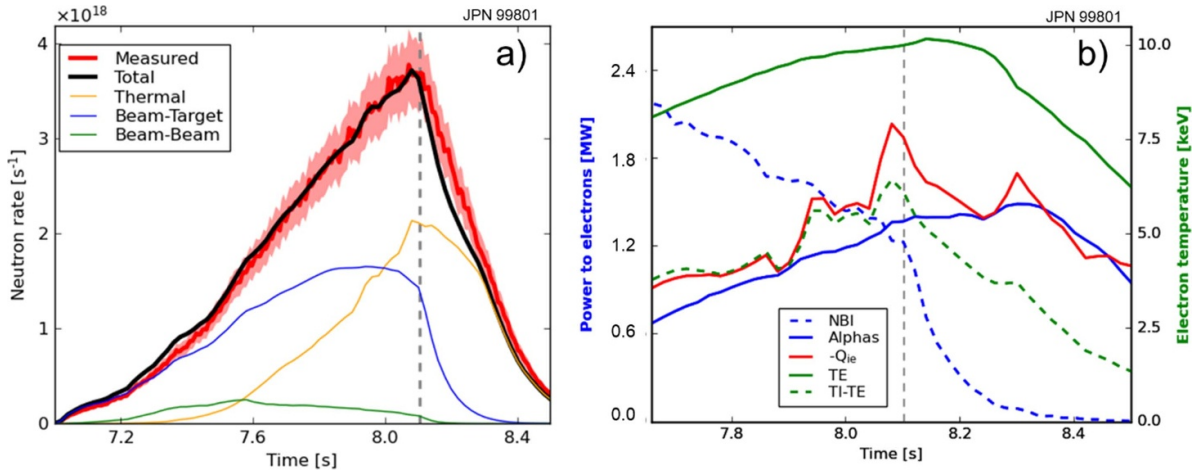

Figure 2. (*a*)—TRANSP neutron rate modelling of JET D-T discharge #99801; (*b*)—TRANSP analysis of electron heating in JET D–T discharge #99801; the power transferred to electrons (left scale) by alphas, NBI and thermal ions (-Qie) are presented as well as electron temperature on axis (TE) and a difference between the ion and electron temperatures (TI-TE) in the plasma core (right scale); the vertical dash line indicates the start of the afterglow.

of electron friction during 400 ms of the afterglow, the average α-particle energy loss is ∼1.8 MeV, so their energy will be $E_\alpha \sim 1.7$ MeV $\gg E_{\rm crit}$. Therefore, *D–T* α-particles can provide a sustainable electron heating during slowing down in the afterglow. The NBI ion thermalisation time is less than 100 ms.

It is important to note that the measured electron density ($n_{\rm e}$) and $T_{\rm e}$ radial profiles at the peak of the *D–T* fusion performance and in the afterglow are changing coherently. We found that in similar pulses without afterglow, the $n_{\rm e}$ density in the plasma core is still rising during $t \approx 8.1$–8.3 s as a result of the transition to H-mode at around 7.2 s. Therefore, it is expected that the $n_{\rm e}$ rise observed in the initial 100–200 ms of the afterglow since the plasma is still in the end of the H-mode transition phase and heating power is still effectively being supplied by the energetic α-particle population. This is an additional evidence of the α-particle self-heating plasma effect.

During the DTE2 experiments, α-particle losses were routinely measured with the scintillator probe FILD and Faraday Cups (FCs). The analysis of the α-particle losses recorded before the NBI power cut and in the afterglow shows that both the energy and pitch-angle distributions are typical for the classical first-orbit losses in both periods. These measurements confirm that α-particles in the discharge are unaffected by any anomalous transport, which could cause additional losses.

The TRANSP [34] neutron rate calculations [35] (see figure 2(*a*)) show that in the analysed *D–T* discharge the thermal neutron rate dominates during both the high-performance and the afterglow periods, exceeding the beam-target neutron rate component. Note that neutron rates in both *D–T* and deuterium discharges are decreasing during the afterglow periods. However, in the deuterium afterglow, the neutron rate decays about two-fold faster than in the *D–T* afterglow phase. The modelling demonstrates that a sluggish decay of the neutron rate observed in the *D–T* discharge is mostly defined by the thermal neutron rate component. Thus, the α-particle generation is sustained for longer in the afterglow, providing an efficient heating of electrons in the core.

Figure 2(*b*) demonstrates results of TRANSP interpretive modelling of electron heating in the *D–T* discharge. The power transferred to electrons by alphas, NBI and the equipartition power exchange between ions and electrons, $Q_{\rm ie}$, are presented for the plasma core, in the range of the dimensionless radius $\rho \equiv \sqrt{\psi_{\rm tor}^{\rm norm}} < 0.05$, where $\psi_{\rm tor}^{\rm norm}$ is a normalized toroidal magnetic flux. Also, the electron temperature on axis and the difference between the ion and electron temperatures, $\Delta T_{\rm ie} \equiv T_{\rm i} - T_{\rm e}$, in the plasma core are shown. The modelling shows that the α-particle power transfer grows during the NBI heating phase and keep growing ≈200 ms in the afterglow up to ≈1.5 MW. At the same time, the NBI power transfer to electrons is promptly dropping. Also, $\Delta T_{\rm ie}$ is decreasing in contrast to the α-particle power transfer that grows during ≈200 ms. One can see that $Q_{\rm ie}$, the equipartition power exchange between ions and electrons, in the core is comparable to the *D–T* α-particle power transfer contribution.

Thus, the transport modelling is consistent with experimental measurements. The presented direct evidence of α-particle heating, which confirms conclusions of former *D–T* experiments, is crucial for developments of burning plasma reactors.

It is known that energetic particles, which stabilise the ion-temperature-gradient-driven microturbulence, could improve energy confinement. Indeed, our TRANSP calculations reveal that the α-particle pressure at the plasma centre, $\rho < 0.05$, is growing up in the heating period and beginning of the afterglow; it is reaching ≈12% of the thermal pressure in the high-performance and afterglow period. Also, the energy confinement time ($\tau_{\rm E}$) being higher than in the reference deuterium discharge is a bit higher or the same (considering experimental uncertainties) in a short period during the afterglow where the α-particle heating was identified. So, figure 3 shows that the value of the fusion triple product, $n_{DT}(0)^*\tau_{\rm E}{}^*T_{\rm i}(0)$, is nearly

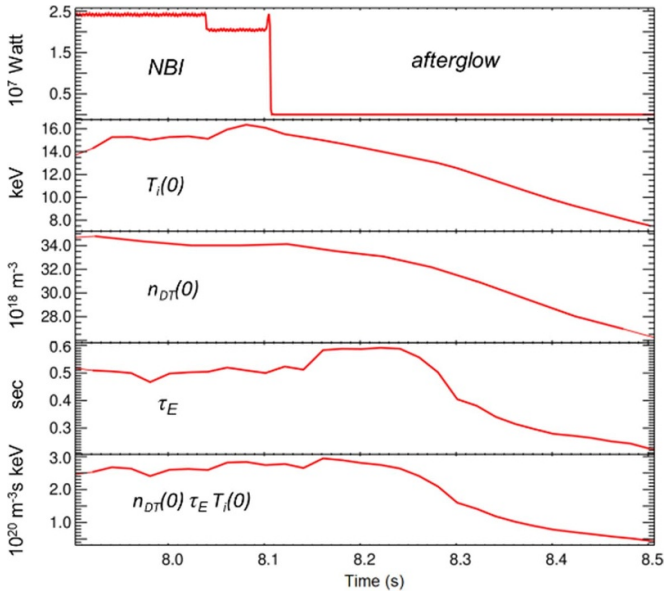

Figure 3. Waveforms of JET discharge #99801 with NBI afterglow: NBI power, central ion temperature and fuel density, total energy confinement time and calculated fusion triple product.

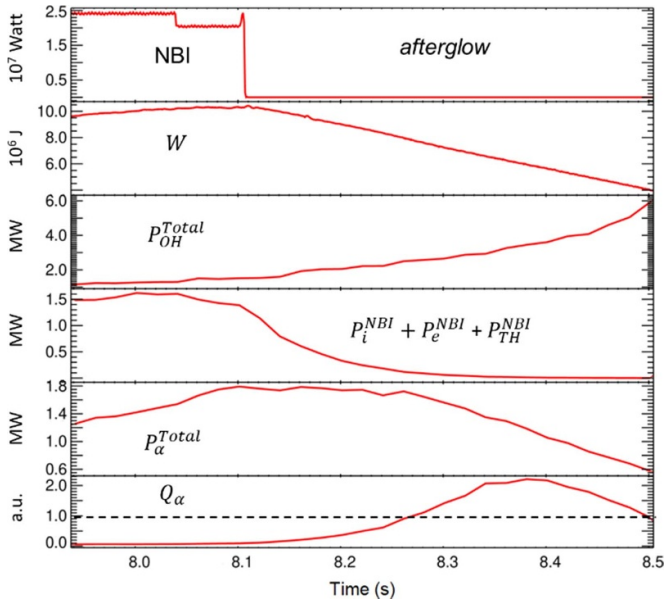

Figure 4. Waveforms of JET discharge #99801 with NBI afterglow: NBI power and plasma energy, W; TRANSP waveforms: $P^{\mathrm{NBI}}{}_{\mathrm{e}}$, $P^{\mathrm{NBI}}{}_{\mathrm{i}}$ and $P^{\mathrm{NBI}}{}_{\mathrm{TH}}$—beam power transfer to electrons, ions and thermalization; $P^{\mathrm{Total}}{}_{\alpha}$—total fusion power to plasma, Q_α—fusion α-particle amplification factor (see text); dash line—$Q_\alpha = 1$ level.

constant ≈3*10^{20} m^{-3} s keV during ≈150 ms, however it is much less that 5*10^{21} m^{-3} s keV required for 'ignition'.

Note, the NBI afterglow *D–T* plasma resembles a self-sustained plasma in a fusion reactor with α-particle only heating. In the absence of any heating sources in JET discharge #99801 (see figure 4), the plasma with energy, W, cools down as $\mathrm{d}W/\mathrm{d}t = -W/\tau_{\mathrm{E}} \approx -16.5$ MW. In the fusion reactor, the power balance for steady-state with α-particle heating (P_α) should be $P_\alpha - W/\tau_{\mathrm{E}} = 0$ but during the afterglow period $P_\alpha < 2$ MW, so it is rather far away from the steady-state power balance. Nevertheless, using parameters obtained with TRANSP (see figure 4), we could assess the afterglow fusion performance with the transient value of the fusion amplification factor after the NBI power cut. There is a definition of the fusion power gain [4] as $Q_{DT} = P_{DT}/P_{\mathrm{in}}$, where P_{DT} is total fusion power (neutrons and alphas) and $P_{\mathrm{in}} = P_{\mathrm{OH}} + P_{\mathrm{NBI}} + P_{\mathrm{ICRF}}$ is total input power to the torus (NBI, ICRF and ohmic). Since in our afterglow case $P_{\mathrm{NBI}} = P_{\mathrm{ICRF}} = 0$, the total ohmic power input P_{OH} is the only one in the denominator for the ratio Q_{DT}. However, the beam-ion power transfer during slowing down in the afterglow should be included i.e. $P^{\mathrm{NBI}}{}_{\mathrm{e}}$, $P^{\mathrm{NBI}}{}_{\mathrm{i}}$ and $P^{\mathrm{NBI}}{}_{\mathrm{TH}}$ are the beam power transfer to electrons, ions and thermalised power of NBI ions. So, in the afterglow we infer the fusion α-particle gain, which is 20% of Q_{DT}, i.e. $Q_\alpha = P^{\mathrm{Total}}{}_{\alpha}/(P_{\mathrm{OH}} + P^{\mathrm{NBI}}{}_{\mathrm{e}} + P^{\mathrm{NBI}}{}_{\mathrm{i}} + \mathrm{P}^{\mathrm{NBI}}{}_{\mathrm{TH}})$, where $P^{\mathrm{Total}}{}_{\alpha} = P^{\alpha}{}_{\mathrm{e}} + P^{\alpha}{}_{\mathrm{i}} + P^{\alpha}{}_{\mathrm{TH}}$ is a total fusion α-particle power transferred to the plasma. Figure 4 shows that Q_α is reaching a maximum value ≈2.2 during the afterglow at 8.35–8.4 s, which is related to the maximum α-particle heating power ≈1.8 MW including power to both plasma electrons (see figure 2(*b*)) and ions.

As one is defined, the self-heating plasma with $Q_\alpha > 1$ is burning. The afterglow self-heating in DTE2 provides the fusion α-particle amplification that exceeds it, $Q_\alpha \approx 2.2$. So, the study of the afterglow plasmas could help to reveal the burning plasma effects in support of the future ITER experiments.

4. Confined alpha-particles

It is a big challenge to measure confined α-particles in the *D–T* fusion plasma. There are several diagnostic problems. The first one is an extremely high expected γ-ray loading of detectors. On JET, during preparation for DTE2, the fast scintillator detectors with effective neutron attenuators were installed and the high-performance data acquisition was developed that has allowed recording of γ-ray spectra at MHz count-rates. Nevertheless, 4.44 MeV gammas of the $^9Be(\alpha,n\gamma)^{12}C$ reaction were not found in the tangential spectrometer spectra, which field-of-view lies ∼30 cm below the plasma centre. It is expected that this γ-ray peak is obscured by the high-level background. The second and most important obstacle for α-particle diagnosing is the 4.44 MeV γ-ray background emission due to the neutron inelastic scattering on the carbon-containing materials, $^{12}C(n,n_1\gamma)^{12}C$. Neutrons with energy exceeding 5 MeV produce these unwelcome background γ-rays. To avoid this background emission, the *LiH* neutron attenuators have been placed in collimators. However, the line-of-sight of the vertical spectrometer intersects the divertor, which is thick CFC tiles covered by tungsten (*W*-CFC), that is why a high 4.44 MeV background γ-ray emission is expected. Figure 5 represents a recorded γ-ray spectrum with a strong 4.44 MeVpeak, which is related to γ-rays due to

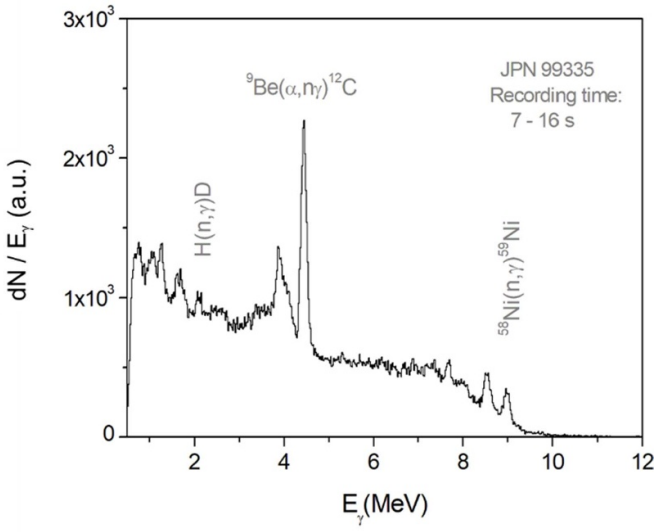

Figure 5. Gamma-ray spectrum (counts per 21 keV) recorded in the JET D–T discharge by the $LaBr_3$ scintillator detector with a vertical line-of-sight; some peaks marked with the related nuclear reactions.

$2^+ - 0^+$ transition of the excited nucleus ^{12}C. This peak contains both the neutron-induced and the confined α-particle components.

Calculations of the γ-ray background emission due to $^{12}C(n,n_1\gamma)^{12}C$ reaction with the General Monte Carlo N-Particle Transport Code (MCNP) [36] reveal that the divertor *W*-CFC tiles generate $\sim 10^{-8}$ γ cm^{-3} per *DT*-neutron. For the vertical collimated detector, the rate is $\sim 7^{*}10^{-13}$ per *DT*-neutron in a typical JET discharge. The γ-ray emission rate produced by α-particles in the JET *D–T* discharges was calculated with the predictive three-dimensional Fokker–Planck modelling code (FIDIT) [37, 38]. The α-particle rate in the field of view of the vertical spectrometer was obtained with the neutron spectrometer, TOFOR [39]. So, the inferred contribution of confined α-particles in the 4.44 MeV γ-ray peak recorded with the spectrometer is ~20%–30% in a typical discharge with 1% Be concentration in the core. In JET plasmas the beryllium contamination varies in the range ~0.5%–1% of n_e and sometimes it is changing due to ELMs during the discharge; therefore, the intensity of the 4.44 MeV γ-ray emission due to alphas can increase. Figure 6 demonstrates the irregularity of this emission, which correlates with the ELM activity. One can see that the neutron rate is uniformly decreasing in the afterglow period of the discharges; however, the 4.44 MeV emission is irregularly increasing due to influx of beryllium.

Furthermore, the high-energy resolution Hp*Ge*-detector was used for measurements of the confined α-particles in discharges with a relatively low *D–T* neutron rate. Figure 7(*a*) shows the Doppler broadened 4.44 MeV peak in the spectra during plasma heating and in extended period including the afterglow. Narrow peaks related to the γ-ray emission of the activated water that was used for neutron detection are

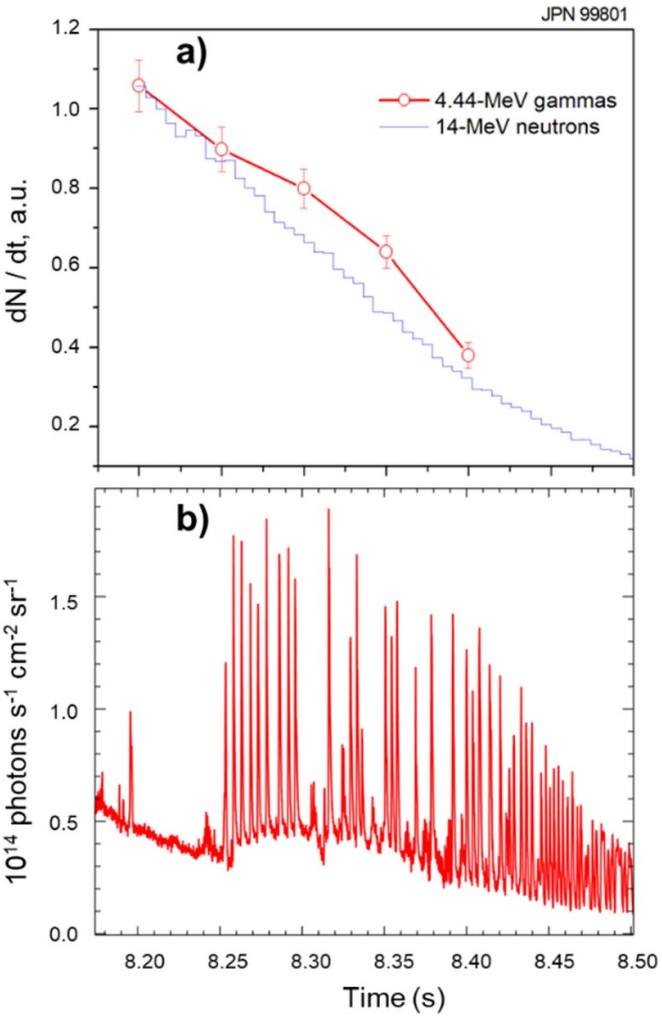

Figure 6. (*a*)—Waveforms of the 4.44 MeV γ-ray FEP and the normalised neutron rate in the afterglow period of D–T discharge; (*b*)—measured photon flux of the beryllium line BeII 527 nm related to the ELM activity.

clearly seen. Note, the response function of any solid-state γ-ray detector consists of the continuous γ-ray Compton scattering spectrum and three peaks: full energy E_γ, single escape (SEP), $E_\gamma - m_e c^2$ and double escape (DEP) $E_\gamma - 2m_e c^2$.

Figure 7(*b*) is a zoomed part of the spectrum, which shows details of the 4.44 MeV peak broadening, and for comparison, the calculated 4.44 MeV peak in the case of the Doppler broadening due to interaction of the MeV α-particles with beryllium impurity. Since the gyro-motion of alphas in the plasma with velocity components in the detector direction and the opposite one, the two-humps peak is observed in the spectrum. In the case of the background $^{12}C(n,n_1\gamma)^{12}C$ reaction the 4.44 MeV peak has a bell-shaped Doppler broadening shape. Hence, it looks like that 4.44 MeV gammas of the $^{9}Be(\alpha,n\gamma)^{12}C$ reaction were mostly detected in the discharge. These measurements confirm the existence of the confined MeV α-particles in the afterglow period for a rather long time.

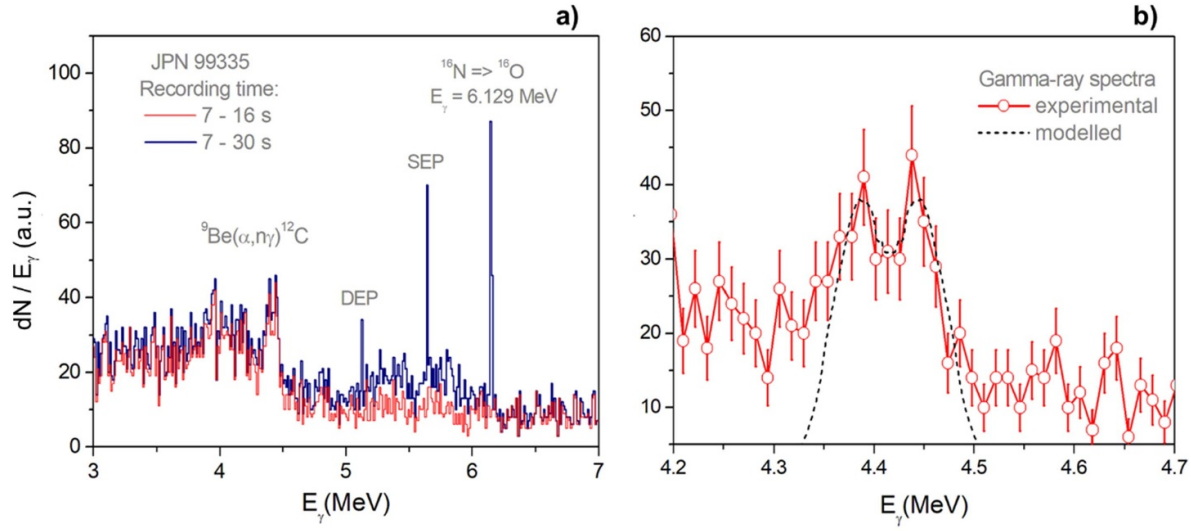

Figure 7. (*a*)—γ-ray spectra (counts per 12 keV) recorded by high-energy resolution HpGe-detector in the JET D–T discharge during the NBI heating period and the period extended to the post-NBI heating phase; (*b*)—part of the spectrum shown in (*a*) and the calculated Doppler broadened 4.44 MeV peak.

5. Alpha-particle losses

5.1. Afterglow α-particle losses

In most high-performance discharges with NBI-only heating with afterglow [40], α-particle losses are of classical first-orbit type, though MHD activity took place before and during the afterglow periods. However, in a couple of discharges during the afterglow phase beginning from $t = 8.055$ s we observed a sharp and massive expulsion of α-particles as shown in figure 8 for the discharge #99870 (3.45 T/2.3 MA). As shown in figure 8(*a*), the α-particle losses in the energy range ≈2.2–2.5 MeV follow the neutron rate and are smoothly decreasing from the NBI power cut. Note, a strong edge localized mode (ELM) at $t \approx 8.085$s does not affect the α-particle losses. Due to the α-particle heating the central electron temperature slightly grows up to the double loss-spike appearing at $t \approx 8.165$s. From this time, T_e is smoothly decreasing in the plasma core ($R \approx 3$ m), however at $R \approx 3.5$ m a sawtooth-like T_e-drop is detected (see a zoom in figure 8(*b*)). Also, about 50 ms later of the first loss spike, there is an ELM activity. A similar effect we observed in discharge #99871 (see a detailed analysis in [41]).

Analysing the Fourier spectrograms of an in-vessel magnetic pickup coil and fast FILD signals, we found that the loss spikes are related to MHD activities. The processed fast FILD signal shown in figure 9 is related to the α-particles in the energy range ≈2.2–3.5 MeV (see the waveform in figure 8). Note that the strong ELM at $t \approx 8.085$s triggered strong $n = 1$ and $n = 2$ modes, however the α-particles have not been affected. The strongest coherent losses are linked to modes $n = 2$ ($f \approx 25$ kHz) and $n = 4$ ($f \approx 125$ kHz) that started in the NBI heating phase and continue in the afterglow. One can see that this α-particle loss coherence disappears due to spike at $t \approx 8.165$ s possibly related to the sawtooth (ST) crash. Furthermore, the $n = 2$ mode dissolves but the $n = 4$ mode frequency is dropping. Also, this event triggered a strong mode $n = 5$ ($f \approx 95$ kHz) and some others. Thus, coherent modes and ST-crash give rise to α-particle transport, a strong redistribution of confined core α-particles, which triggers ELM burst and massive spike losses in the energy range ≈2.2–3.5 MeV. Also, one could suggest non-linear effects which have not been examined but may be present here.

To confirm this α-particle effect, we have selected FILD losses related to the spikes, separating them from the continuous losses. This differential footprint (peak losses minus the continuous signal) of α-particle losses detected by CCD is shown in figure 10. One can see a hot-spot of losses in the gyro-radius and pitch-angle ranges, $r_{gyr} \approx 8-10$ cm and $\theta \approx 50°-55°$. The calculated orbits, which are related to the represented loss footprint, show that the lost α-particles at $t \approx 8.165$ s intersect a broad area at $R \approx 3.2$–3.5 m that includes the $q = 1$ surface.

5.2. Fishbone α-particle losses

During the development of a high-performance hybrid *D*-plasma scenario for DTE2, an increased level of *D*–*D* fusion product non-resonant losses, tritons and protons, in the MeV-energy range was observed during the instability of $n = 1$ fishbones [26]. The fishbones were excited during *D*-NBI combined with ICRF heating. The frequency range of the fishbones, 10–25 kHz, indicates that they are driven by a resonant interaction with the NBI-produced *D*-beam ions in the energy range ⩽120 keV. It was found that spatial redistribution of the NBI-ion population can be caused by the fishbones [42]. The experimental observation and modelling [43] of the non-resonant losses of *D*–*D* fusion products caused by low-frequency fishbones confirmed the loss mechanism proposed in [44].

In DTE2, it was also found that α-particle losses are coherent with fishbones. A strong fishbone activity was observed

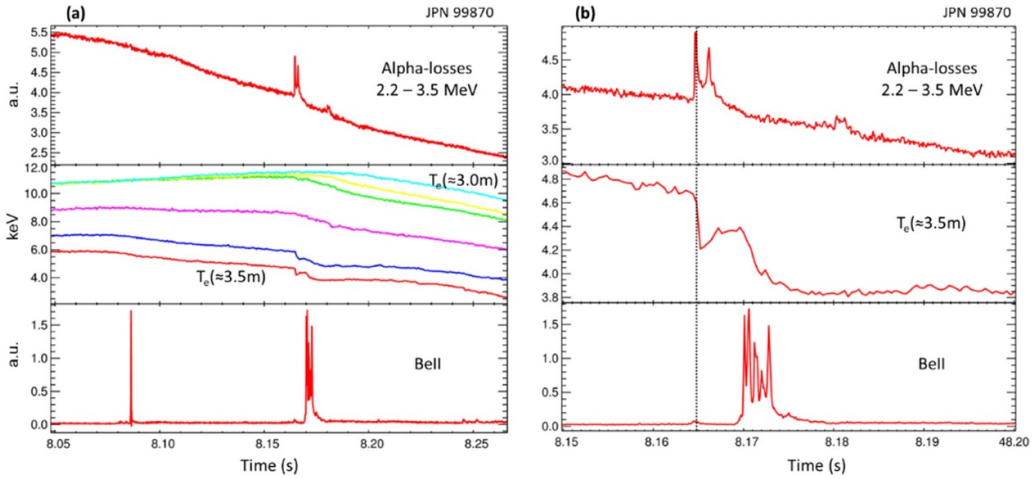

Figure 8. Waveforms of JET discharge #99870 (afterglow from 8.055s); (*a*)—FILD-SP output signal (a.u.) related to α-particle losses in the range ≈2.2–3.5 MeV, the ECE electron temperature mapped onto the magnetic axis from $R \approx 3.0$–3.5 m and BeII 527 nm photon flux related to the ELM activity; dash-line marks the time of the NBI power cut; (*b*)—a zoom of the time-window with loss spikes; the dot-line marks the first loss-spike.

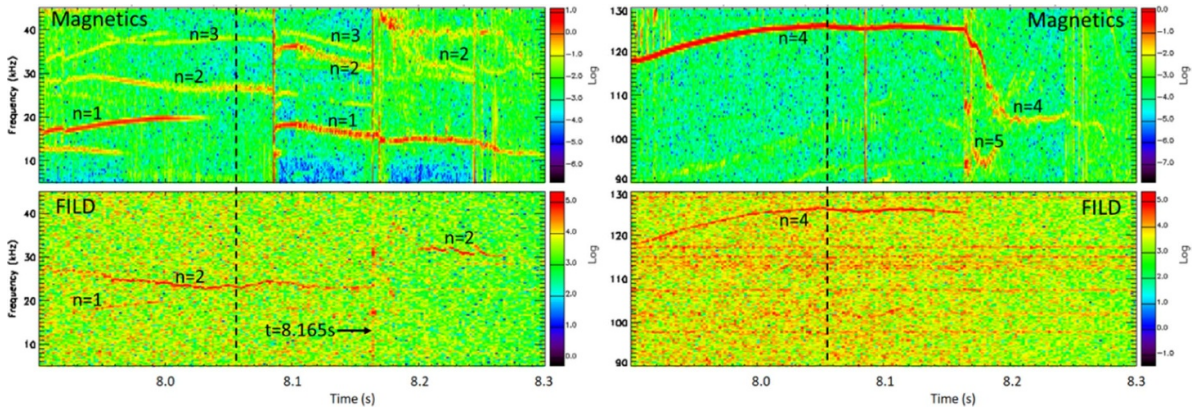

Figure 9. Fourier spectrograms of an in-vessel magnetic pickup-coil (upper boxes) and FILD (bottom boxes) signals detected in JET discharge #99870; left boxes—frequency range 5–45 kHz, right boxes—frequency range 90–130 kHz; vertical lines indicate beginning of the afterglow period.

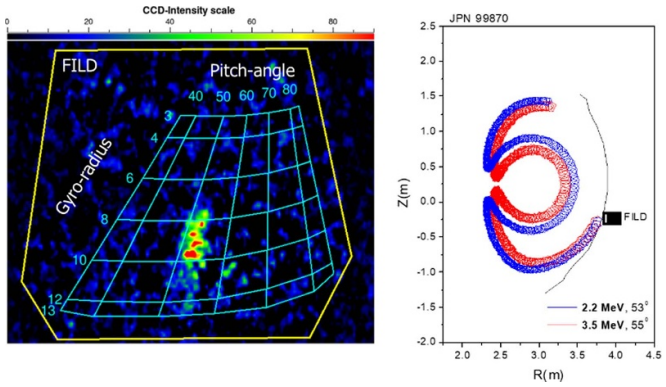

Figure 10. A differential footprint of α-particle losses detected by FILD CCD in JET discharge #99870 at $t \approx 8.165$ s, which is related to losses in the energy range ≈2.2–3.5 MeV; the lost α-particle orbits calculated back-in-time from the footprint.

in both the hybrid [30] and the baseline H-mode scenario [45] discharges. The high-performance hybrid pulse #99950 (see waveforms in figure 11(*a*)) produced total fusion energy of ≈45.8 MJ with $n_D \approx n_T$ plasma even though a strong $n = 1$ fishbone activity continued for ∼2 s, increasing from $t \approx 9$ s. Alpha-particle losses detected with FILD dominate (see figure 11(*a*)), however there are low-energy ions (slow alphas and NBI-ions) that are lost due to the strong

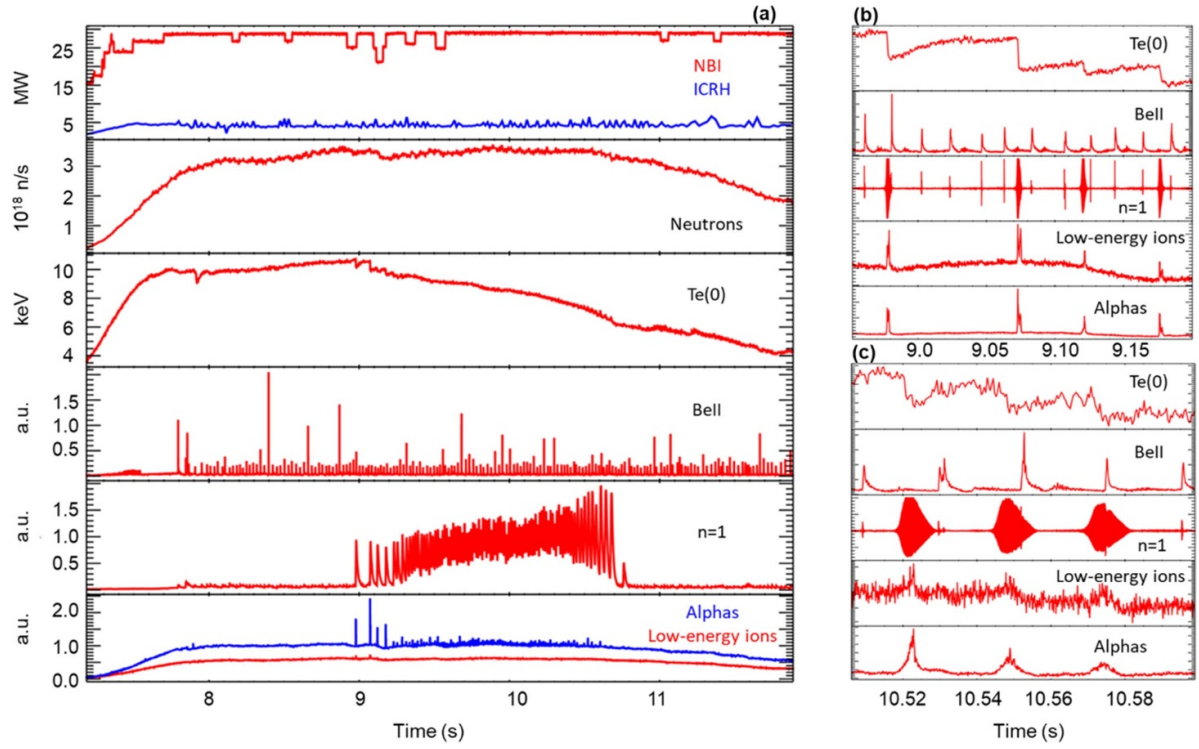

Figure 11. Waveforms of JET discharge #99950(3.4 T/2.3 MA): (*a*)—NBI and ICRF power, neutron rate, central T_e, BeII photon flux used for ELM timing with ITER-like wall, the in-vessel magnetic pickup-coil signal related to $n = 1$ and FILD signal related to the fast α-particle and low-energy ion losses; (*b*), (*c*)—two zoomed time slots.

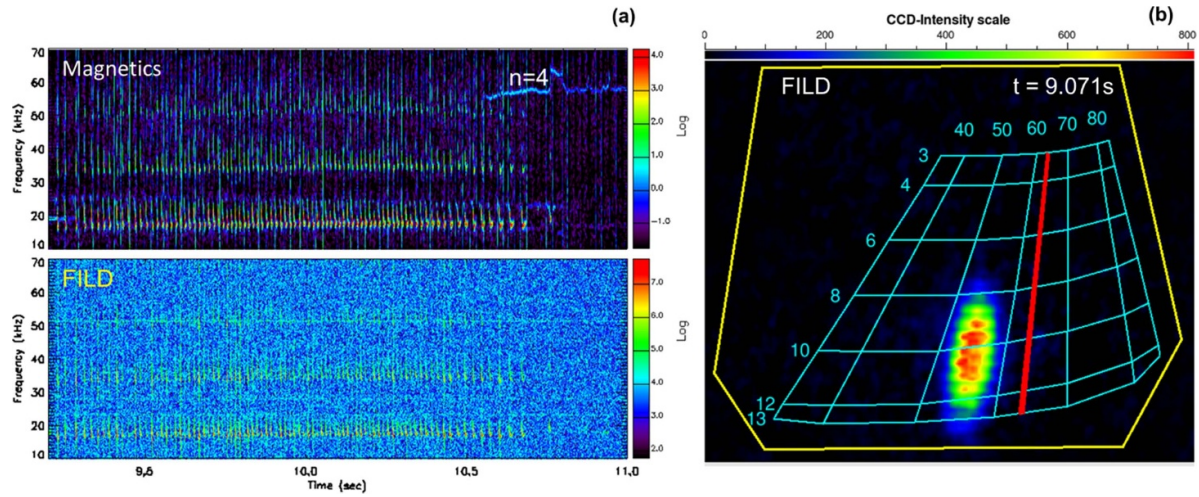

Figure 12. (*a*)—Fourier spectrograms of an in-vessel magnetic pickup-coil (upper box) and FILD (bottom box) signals detected in JET discharge #99950; (*b*)—footprint of α-particle losses detected by FILD CCD in JET discharge #99950 at $t \approx 9.071$s; red-line indicates the ICRF resonance layer on the grid.

sawteeth reconnections trigged by the $n = 1$ fishbones shown in figure 11(*b*). Losses at the end of the strong fishbone activity are shown in figure 11(*c*). The Fourier analysis reveals that α-particle losses are coherent with fishbones (see in figure 12(*a*)), confirming our past observations of the fusion product losses. It was found that the fishbone induced losses are related to alphas with energies more than 2 MeV. An example of the FILD footprint of alphas due to the fishbone at $t = 9.071$ s is demonstrated in figure 12(*b*). The back-in-time calculation of orbits shows that α-particles came from a trapped-passing boundary phase-space. Note, these strong fishbones and related losses cause the sawteeth and the continuous core T_e decrease. Meanwhile, the fishbones do not affect the fusion performance since the neutron rate grows up to $t = 10.55$ s, when a tearing mode with toroidal number $n = 4$ is triggered by a strong ELM (see upper box in figure 12(*a*)).

A similar fishbone effect has been observed in the baseline H-mode scenario JET discharge #99948 (3.3 T/3.5 MA) [45] presented in figure 13. One can see that regardless of a long fishbone activity started at $t \approx 9$ s the neutron rate is

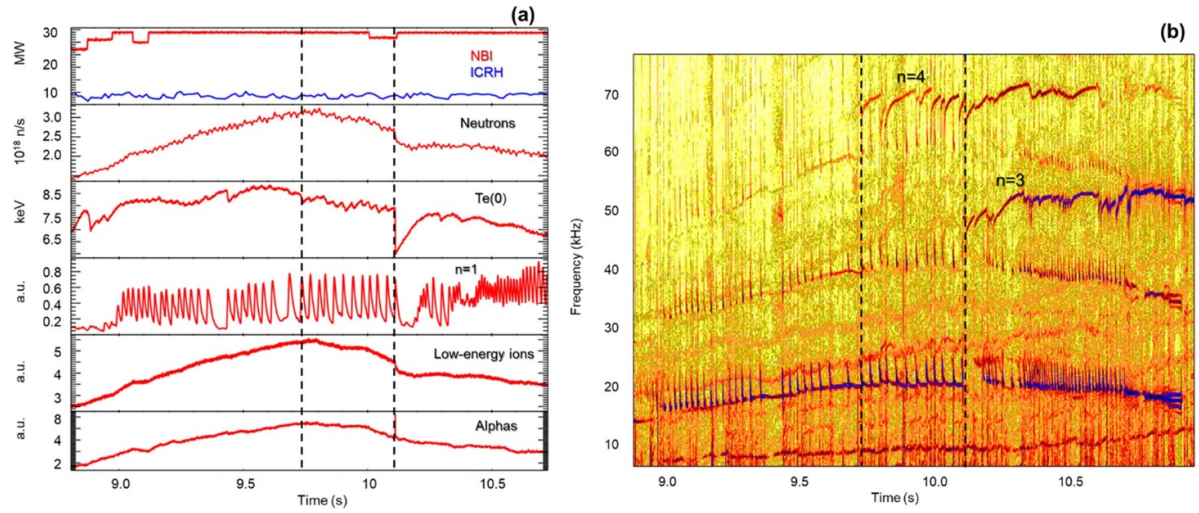

Figure 13. (*a*)—waveforms of JET discharge #99948 (3.3 T/3.5 MA): NBI and ICRF power, neutron rate, central T_e, the in-vessel magnetic pickup-coil signal related to $n = 1$ and FILD signal related to the fast α-particle and low-energy ion losses; (*b*)—Fourier spectrogram of an in-vessel magnetic pickup-coil.

continuously growing up to appearance of a strong $n = 4$ continuous mode (see figure 13(*b*)). The central T_e is increasing as well but sawtooth-like crashes triggered by fishbones restrict the growth. This fishbone sequence is interrupted by a monster sawtooth, which triggered $n = 3$ continuous mode. Note, losses in this discharge follow the neutron trend that is an indication of a classical prompt escape from the plasma. However, the monster sawtooth crash caused a spike of the α-particle losses.

In these JET discharges with NBI and ICRF heating the α-particle contribution to the total fusion power is unsubstantial. Therefore, alpha-losses due to fishbones do not affect the fusion performance as the neutron rate indicates. However, the fishbone related α-particle losses can be a problem in the burning plasma with strong α-particle heating and this issue need to be investigated for a specific fusion reactor e.g. ITER, DEMO.

5.3. ELMs and α-particle losses

In the high-performance *D*–*T* discharges we observed α-particle losses correlated with the appearance of ELMs. In discharge #99449 (3.4 T/2.3 MA) presented in figure 14(*a*) one can see strong spikes of the *BeII* emission that indicates ELM activity. The FILD α-particle loss PMT waveform follows the neutron rate one and indicates the first-orbit prompt losses. Nevertheless, there are spikes of losses which are rather strong. Figure 14(*b*) represents a time slice with two ELMs and alpha-loss spikes. Note, the appearance of the first alpha-loss and ELM spikes coincides, see figure 14(*c*). However, the second, the strongest peak of losses is ∼15 ms later than the second ELM.

The scintillator probe FILD measurements can expose the energy range of the α-particle losses. The differential CCD footprints presented in figure 15 show that the first peak of losses is related to α-particles, $E_\alpha \approx 2.2$–3.5 MeV, while the strongest second one indicates less energetic lost alphas, $E_\alpha \approx 1.5$–3.0 MeV. Nonetheless, the range of the lost particle pitch- angles, $\theta \approx 50°$–$54°$, is the same in both cases. The back-in-time orbit calculations presented in figures 15(*c*) and (*d*) demonstrate evidence for α-particles with energies $E_\alpha > 2.5$ MeV passing marginally close to the plasma edge and the alphas would cause ELMs. Note, the ECE diagnostics confirm that the T_e irregularity is localised at $R \approx 3.80$ m. As to the second loss-peak, less energetic alphas were lost from a trapped-passing boundary phase-space. The Fourier analysis indicates that α-particle losses are in coherence with continuous kink modes in this discharge (see figure 16). Thus, in fact instabilities redistribute alphas pushing them in the loss cone. Also, it is curious that in contrast to $n = 2$ and $n = 3$ modes in magnetics spectrogram the related FILD losses are splitting at $t \approx 8.05$ s. However, there is no explanation of this effect unless that is an artifact.

5.4. Anomalous α-particle losses

In special 'bump-on-tail' experiments [46] ($B_T = 3.7$ T, $I_P = 2.5$ MA) anomalous losses of the MeV alphas were observed with FILD SP and FC. The main source of α-particles was of the beam-plasma type due to modulated injection of 110 keV *D*- and *T*-beams ($P_{NBI} \approx 10$–15 MW) in both *T*-rich and *D*-rich L-mode plasmas. Figure 17 shows footprints of α-particle losses recorded with FILD CCD camera in these type discharges.

It is clearly seen that in both cases the pitch-angle distribution of losses has 'double-hump' features. One can see that a maximal loss rate appears at $\theta = \cos^{-1}(v_\parallel/v) \approx 58°$ and $\approx 75°$, whilst minimal losses are in the range $\theta \approx 62°$–$70°$. Since the first orbit losses are of the particles with trapped orbits, the major radius at the bounce reflection point for these particles and the pitch-angle value on the scintillator plate are related by $R(\theta) = R_{FILD}[1–\cos^2(\theta)]$, where R_{FILD} is the radial position of the scintillator plate. So, α-particles originated in the plasma regions near to $R(58°) \approx 2.75$ m and $R(75°) \approx 3.6$ m

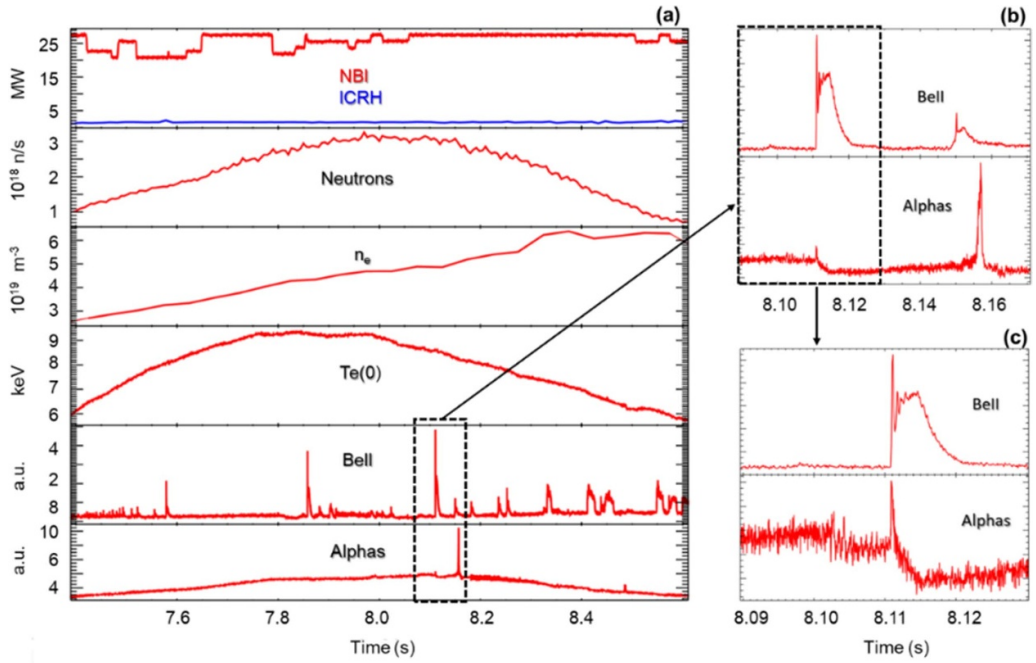

Figure 14. (*a*)—Waveforms of JET discharge #99449 (3.4 T/2.3 MA): NBI and ICRF power, neutron rate, central n_e and T_e, BeII photon flux used for ELM timing with ITER-like wall and FILD signal related to the fast α-particle losses; BeII and α-particle loss signals marked with dash-line box are zoomed in (*b*); (*c*)—zoomed timeslot marked with dash-line box in (*b*).

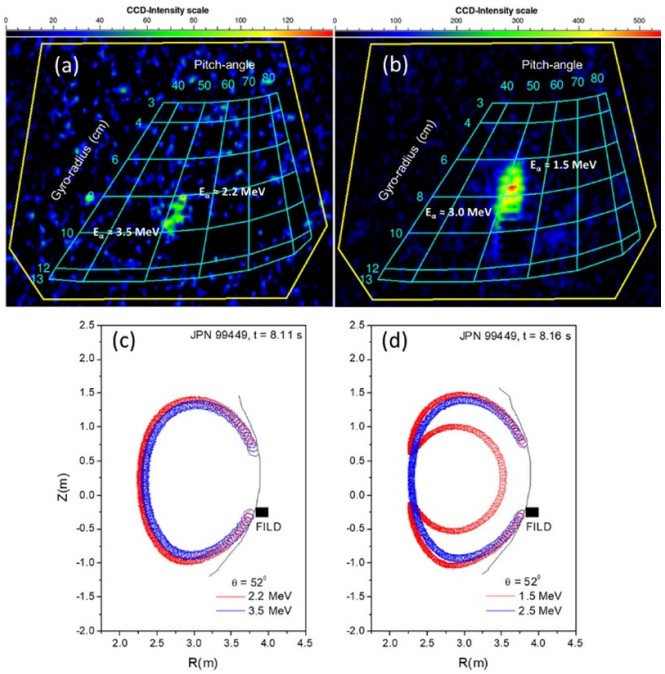

Figure 15. (*a*) and (*b*)—Differential footprints of α-particle losses detected by FILD CCD in JET discharge #99449 at 8.11 s and 8.16 s, accordingly; (*c*) and (*d*)—lost α-particle orbits calculated back-in-time from the footprints (*a*) and (*b*).

have experienced more intensive losses than α-particles from the $R \approx 3.0$–3.3 m, in the vicinity of the magnetic axis that was at $R \approx 3.0$ m. Analysis of interferometry, reflectometry and soft x-ray data indicates high-frequency Alfvénic activity, however no α-particle loss correlations were observed.

An important piece of information was obtained with neutron profile measurements that characterise the α-particle source. Figure 18 represents an example of tomographic reconstruction of the line-integrated *D*–*T* neutron emissivities recorded with the 2D neutron camera. The shown α-particle source profiles are related to the discharge with fuel plasma composition $D(42\%)$:$T(58\%)$ and the central electron temperature and density, $T_{e0} \approx 4$ keV and $n_{e0} \approx 4 \times 10^{19}$ m^{-3}. One can see that the profiles have similar features, a sort of 'shoulders', in both cases. Since the neutron emissivity in this discharge is characterised by a dominant beam-target component, the obtained profiles could point at anomalous transport of the NBI ions that may be a reason for the observed effects in the prompt α-particle loss pattern.

Alpha-particles were studied in the *D*–*T* plasma discharges at $B_T = 3.7$ T, $I_P = 2.5$ MA with a novel ICRF heating scheme—three-ion ICRF heating of naturally present ^9Be-impurity in JET ($f_{ICRF} = 25$ MHz) [47]. Such ICRH scheme, due to the large atomic mass of Be, provided an effective bulk ion-heating in the plasma core and furthermore, without ICRF-driven TAE modes. Surprisingly, the 'double-hump' α-particle loss pattern (see figure 19(*b*)) was also observed in these discharges. Figures 19(*a*) and (*c*) show the 3.5 MeV α-particle orbit calculation launched from the designated areas of the FILD scintillator plate which is related to the humps. One can see that the plasma core region is characterised by a reduced loss rate and that is consistent with the results of the NBI-only experiments discussed above. However, a further surprising effect was observed in the three-ion ICRF heating discharges at $I_P = 2.0$ MA. A comparison of α-particle losses in discharges with $I_P = 2.5$ MA and 2.0 MA is represented in figures 20(*a*) and (*b*).

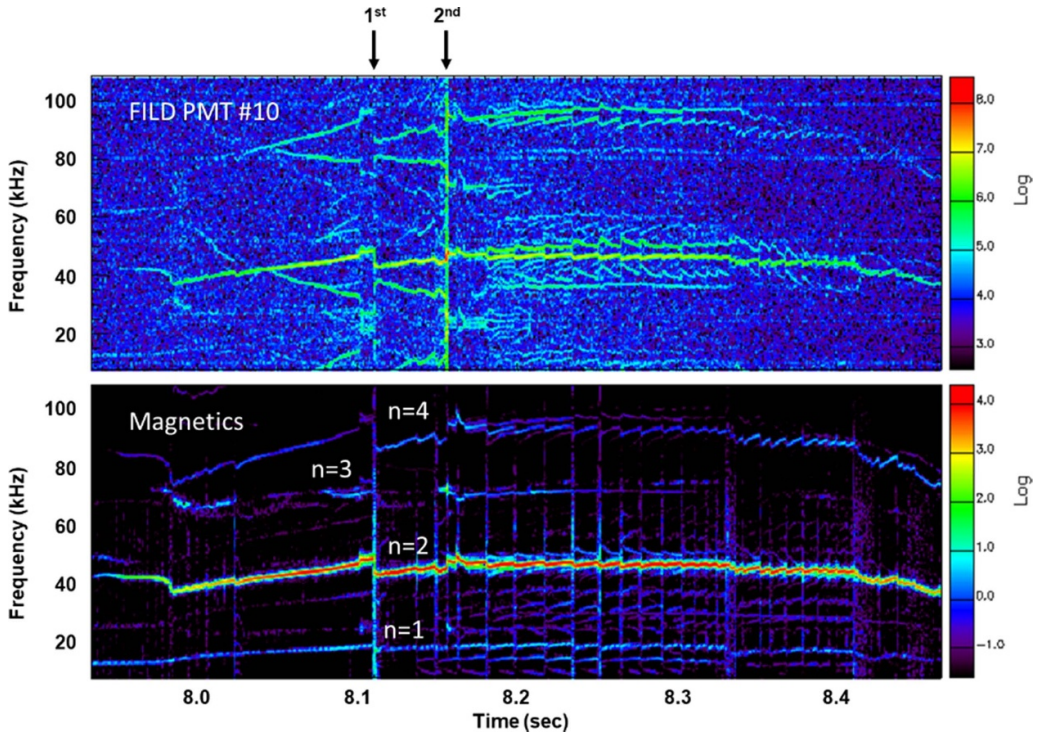

Figure 16. Fourier spectrograms of an in-vessel magnetic pickup-coil (upper box) and FILD (bottom box) signals detected in JET discharge #99449; arrows show when 1st and 2 nd α-particle loss spikes happened.

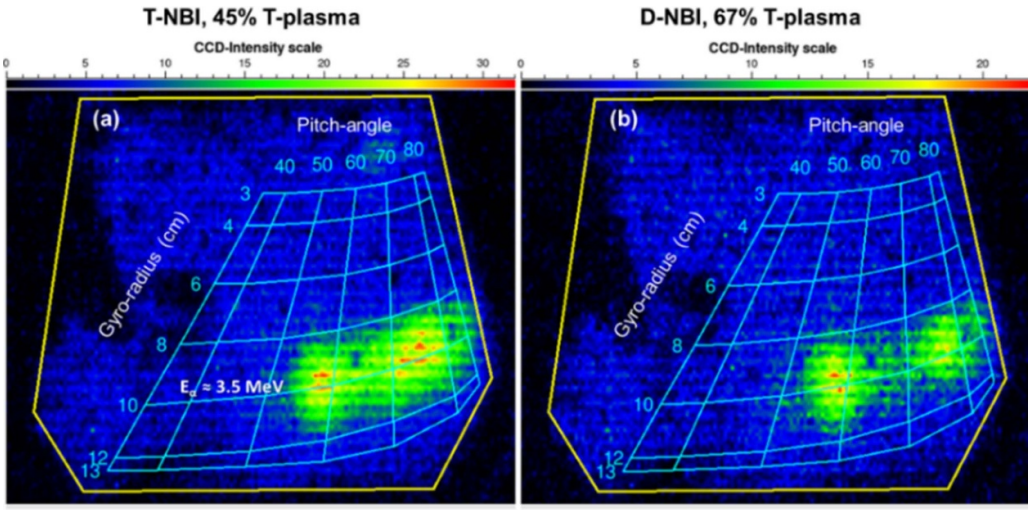

Figure 17. FILD CCD camera images recorded in JET D–T discharges with NBI-heating: (*a*)—JPN 99 502, the signal integrated during 7.20–7.45 s; (*b*)—JPN 99 503, the signal integrated during 8.0–8.5 s.

Since in-vessel magnetic pickup-coils indicated relatively low MHD activity in both discharges, perhaps any anomalous transport does not explain the α-particle anomalous losses. Furthermore, nearly identical neutron profiles (see figure 20(*c*)) confirm both an effective central heating of plasmas with three-ion ICRF scheme and lack of difference in the NBI-ion transport.

Note that the double hump losses have been observed in special ripple experiments on JET [48]. Also, anomalous losses of *D–D* fusion tritons and protons have been observed in some JET plasmas with normal ripples which are very low. Modelling of these discharges demonstrated that fusion products may experience a super-banana diffusion, which is significantly exceeding the neoclassical level [49].

Thus, MHD or/and anomalous transport could push α-particle to ripple trapping. The physics behind this anomalous α-particle losses is being investigated.

In this section, several experimental observations and measurements of α-particle losses in DTE2 discharges have been highlighted. Additional information on alpha-losses can be also found in [41] and [50].

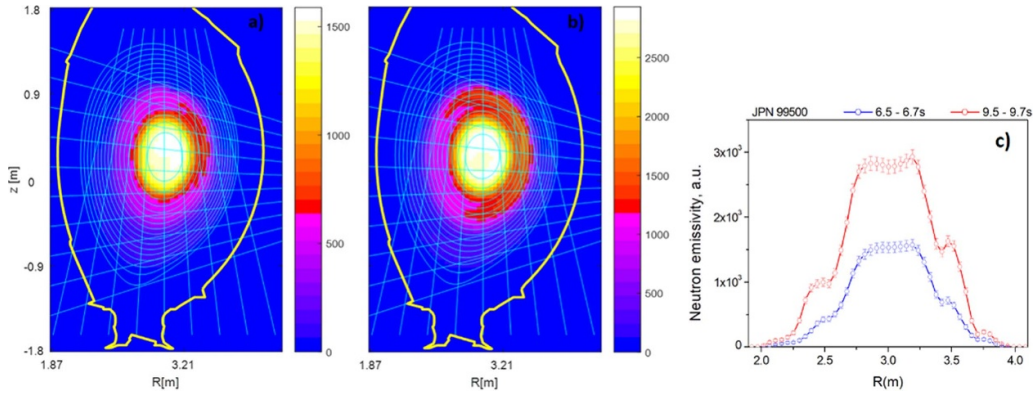

Figure 18. 2D tomographic reconstruction of the D–T neutron emissivity obtained with 2D neutron camera for JET discharge #99500: (*a*) period of T-NBI heating during $t = 6.5$–6.7 s, (*b*) D-NBI heating during $t = 9.5$–9.7 s; the colour scale is normalised; (*c*)—reconstructed midplane neutron emissivities during T- and D-NBI heating periods.

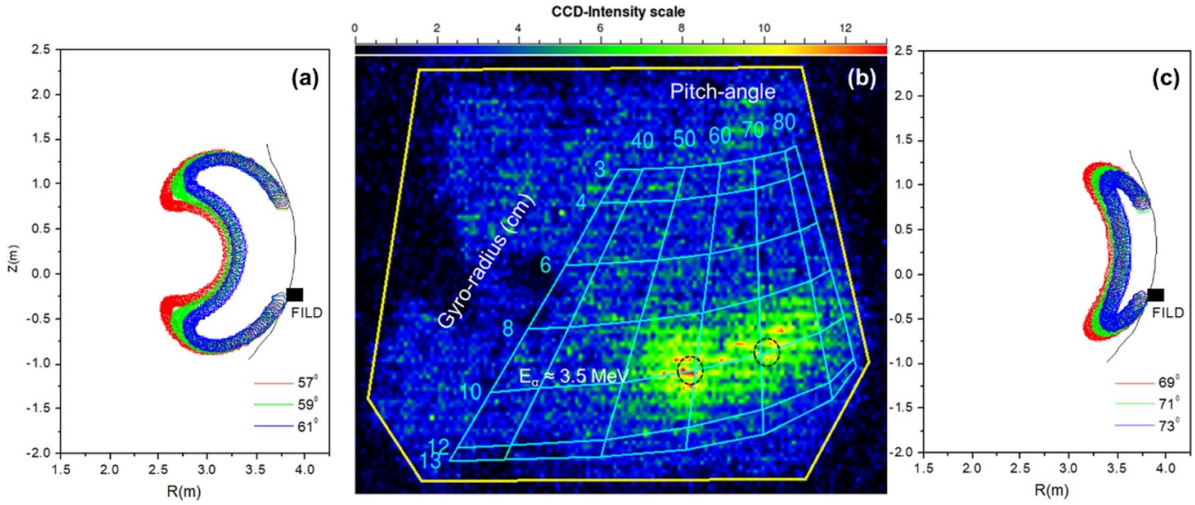

Figure 19. FILD CCD camera image (*b*) recorded in the 2.5 MA discharge JPN 99 604 with three-ion ICRF heating (integration time 10.5–10.6 s) and lost 3.5 MeV α-particle orbits calculated back-in-time from the loss footprint (black dash circles); (*a*)—orbits related to pitch-angles 57°–61°; (*c*)—orbits related to pitch-angles 69°–73°.

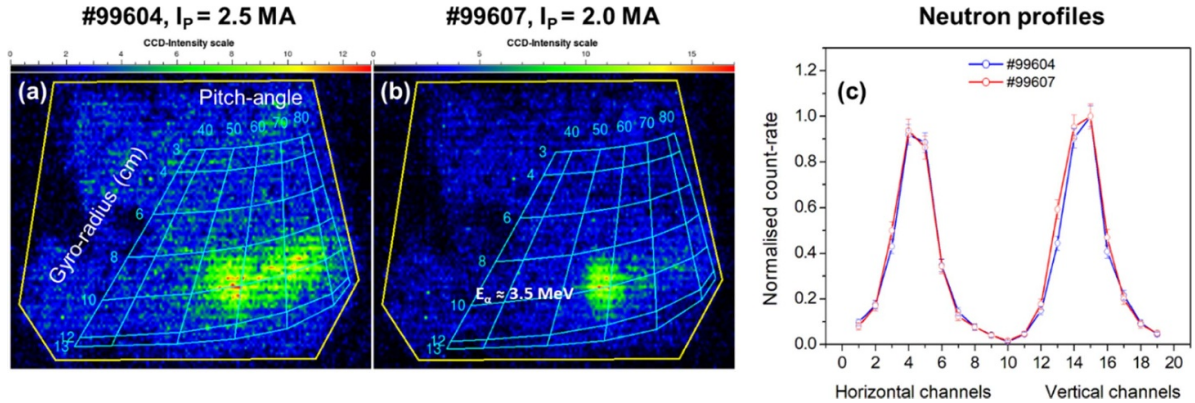

Figure 20. FILD CCD camera images recorded in discharges with three-ion ICRF heating (integration time 10.5–10.6 s): (*a*)—discharge JPN 99 604, $I_P = 2.5$ MA; (*b*)—discharge JPN 99 607, $I_P = 2.0$ MA and a comparison of the D–T α-particle source profiles measured with neutron camera in these discharges.

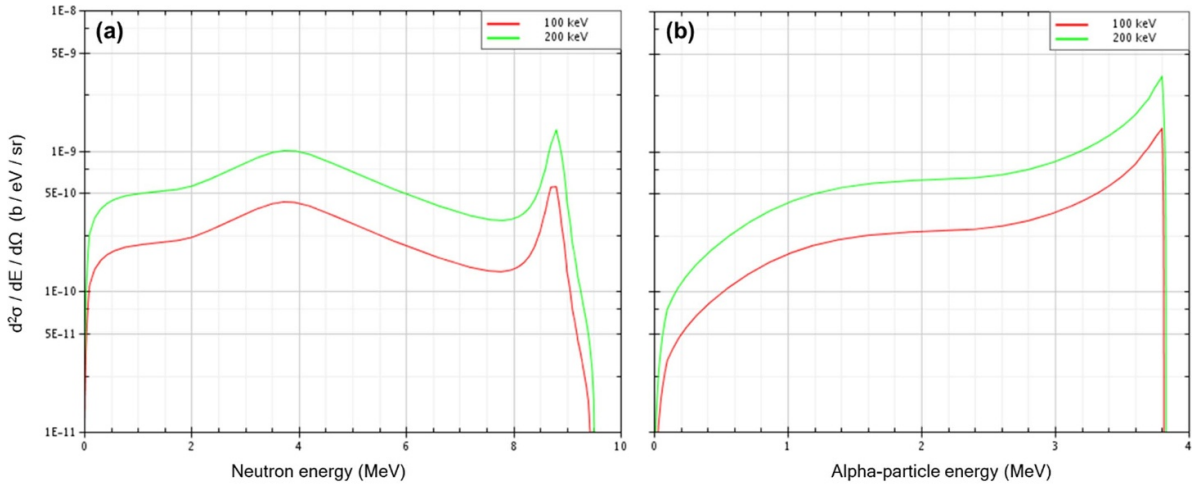

Figure 21. Forward angle energy spectra of the $T(T,2n)^4$He reaction products calculated for 100 keV and 200 keV T-beams [54]: (*a*)—neutrons; (*b*)—α-particles.

6. Alpha-particles in tritium plasmas

An important part of the fusion-born α-particle studies on JET took place in the 100% tritium plasma experiments. The α-particle spectrum in tritium plasmas is rather complicated because there are several branches of the *T*–*T* fusion. Indeed, the $T(T,2n)^4He$ reaction gives rise to neutrons and MeV α-particles with continuous energy spectra since three outgoing particles in the final state providing ~70% of the total *T*–*T* reaction rate. The maximal energy of the *T*–*T* neutrons is about 9 MeV, whereas α-particles are born in the energy range $E_\alpha \approx 0$–3.8 MeV. In addition, a contribution ~30% of monoenergetic alphas due to the sequence of the $T(T,n)^5He$ reaction followed by a decay $^5He \rightarrow n + {}^4He$ is present. For the MeV-tritons the angular distribution of the α-particles is predominantly forward and backward along the direction of motion of the ^5He nucleus [51], and thus the energy spectrum is peaked at both the maximum and minimum energies. However, the in-beam experiments with 220 keV tritons [52] indicate that contribution of this reaction branch is much less than the three-particle one. Theoretically, the neutron and α-particle spectra can be approximated using a model [53]. An example of the calculated neutrons and α-particle spectra [54] is presented in figure 21. Note, the cross-section of the $T(T,2n)^4He$ fusion reaction is continuously increasing with triton energy.

It is important to emphasise, that since the broad energy-range of the *T*–*T* fusion α-particles, their interaction with plasma differs from the *D*–*T* 3.5 MeV alphas. The critical energy for α-particles $E_{crit} \approx 0.4$ MeV, therefore the MeV *T*–*T* alphas are heating electrons as we have observed in *D*–*T* plasmas. At the same time, the *T*–*T* alphas being born at $E_\alpha < E_{crit} \approx 0.4$ MeV mostly interact with bulk *T*-ions. Thus, both alphas and 110 keV *T*-beam ions (because for tritons $E_{crit} \approx 0.3$ MeV) are heating plasma ions. There are two groups of energetic tritons that produce neutrons and alphas: injected 110 keV *T*-beam ions and a population of energetic bulk tritons which is generated due to a collisional α-particle thermalisation. Note, modelling of the *T*–*T* neutron rate with TRANSP in the *T*-plasma discharges is not adequate as the α-particle differential cross-sections, $d^2\sigma_\alpha^{TT}/dE_\alpha/d\Omega_\alpha$, is not implemented in the code yet.

Alpha-particle losses have been studied in the high-performance *T*–*T* plasma discharges. In figure 22(*a*) the FILD footprint of losses recorded in hybrid discharge #99151is shown. There are two spots of losses on the scintillator plate which are presumably related to α-particles. The high-energy losses are spotted within gyro-radius $r_{gyr} \approx$ 8–12 cm, the low-energy loss spot lie at $r_{gyr} < 4$ cm. The energy distribution function of α-particle losses obtained by integrating the CCD output along $\theta = 60^\circ$ with a subtracted background is presented in figure 23. This distribution has a broad peak at ≈4 MeV and strong low-energy losses $E_\alpha < 1$ MeV. A reverse-time α-particle orbit calculation started from the hot spots in figure 22(*a*) show that energetic alphas are leaving the plasma core whereas low-energy ions are lost from the periphery. These observations confirm the strong angular-distribution of *T*–*T* α-particles and can be used for studies of the $T(T,2n)^4He$ reaction features that is important for astrophysics. However, to obtain the α-particle loss distribution a deconvolution of the CCD output is needed considering the FILD response function, which has a strong gyro-radius dependence [24, 25]. The analysis of this interesting observation is in progress.

Also, it was found that the fast signal recorded by PMT#10, which is viewing the designated area, is coherent with an $n = 2$ mode (see spectrograms in figure 22(*b*)), which according to waveforms shown in figure 22(*d*), is triggering a strong ST-crash at $t \approx 7.81$ s and α-particles in the energy range 2.2–4.2 MeV were pushed off from the plasma centre. One can see in figure 22(*d*) that the central electron temperature, $T_e(0)$ is continuously decreasing after the ST-drops though the neutron rate is still increasing. So, low-energy ions with energy below 0.3 MeV, which mostly heat ions, are not affected by ST-crash that is confirmed by the PMT#03 and PMT#04 waveforms. However, these waveforms have spikes which exactly coincide

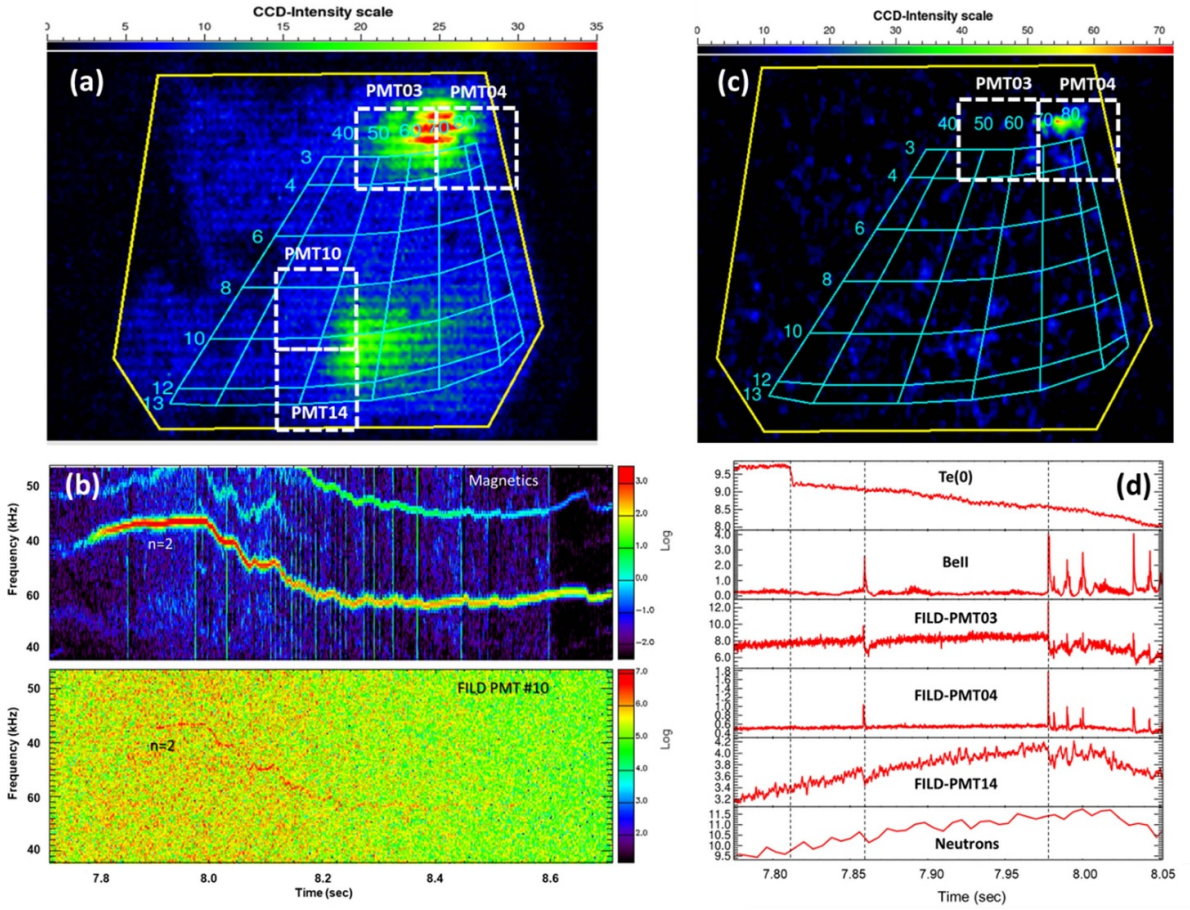

Figure 22. TT-discharge #99151: (*a*)—FILD CCD camera image recorded during $t = 7.8$–7.9 s; PMT fields of view marked with white rectangles; (*b*)—Fourier spectrograms of an in-vessel magnetic pickup-coil (upper box) and FILD PMT#10 (bottom box); (*c*)—differential image of the FILD CCD camera recorded at $t = 7.977$s; (*d*)—waveforms of the discharge; dashed lines marks times of a sawtooth and spikes of BeII photon flux used for ELM timing in JET with ITER-like wall.

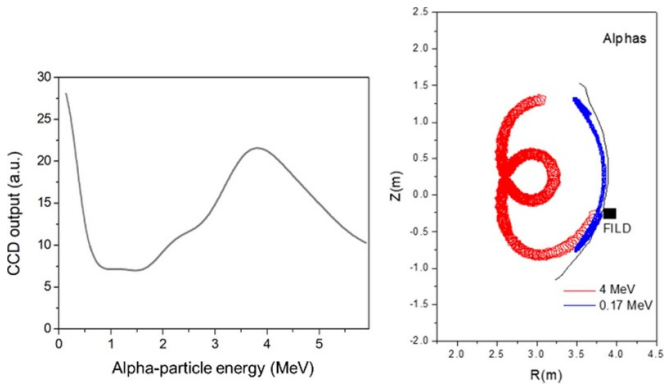

Figure 23. TT-discharge #99151: energy distribution function of α-particle losses obtained by integrating the CCD output along $\theta = 60^\circ$ (left box); alpha-particle orbits calculated back-in-time from the FILD (right box).

with some spikes in the *Be*II-photon emission related to ELMs. Note, the PMT#04 spikes are much stronger than spikes in the PMT#03 waveform. Furthermore, there is a drop of the loss signal with a relaxation after each ELM that could mean a reduction of the *T*–*T* α-particle production due to *T*-beam ion loss. This explanation is fully confirmed by the differential footprint of losses shown in figure 22(*c*), which is a difference between the signal of the CCD frame recorded with ELM and the frame before it.

The bright spot on the scintillator is relevant to $E_T \sim 60$ keV (also, it can be $E_\alpha \sim 180$ keV), which could be a half-energy fraction of the 120 keV *T*-beam. An additional confirmation of the *T*-beam losses due to ELMs is the signal drop in the PMT#14 waveform, which is related to the high-energy α-particle losses. As a result of this analysis, one can conclude that losses of energetic alphas are coherent with low-frequency long-lasting MHD modes, whereas some low-energy *TT*-alphas and *T*-beam ions are lost at the plasma periphery and can be affected by ELMs.

7. Fusion gamma-ray measurements

The radiation capture reactions are unique for the fusion rate monitoring in the case of *D*–*T* and aneutronic fusion i.e. *D*–*H, T*–*H* and ^{3}*He*-*D,* or advanced fuel scenarios such as *Li*–*H* and *B*–*H* [11]. Also, some of these reactions, for an example *D*–*H* and *T*–*H* fusion, could be used for measurements of both temperature and fuel ratio in the plasma core [19, 55].

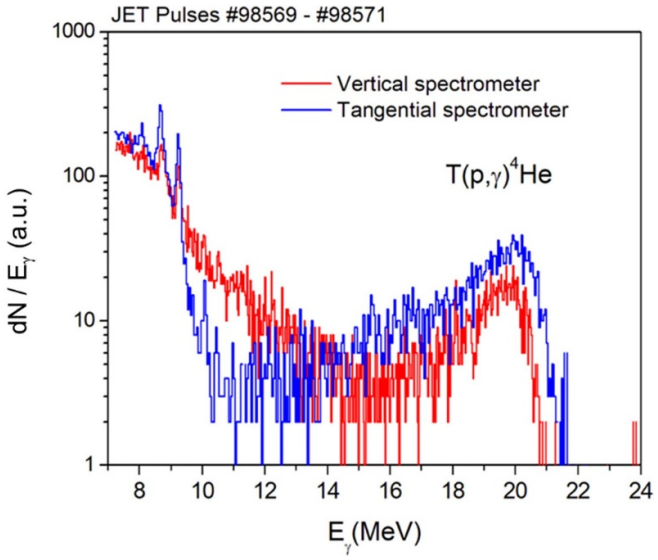

Figure 24. Integrated γ-ray spectra (counts per 47 keV) recorded by $LaBr_3$-detectors with vertical and tangential lines of sight in the T-plasmas with H-minority heating.

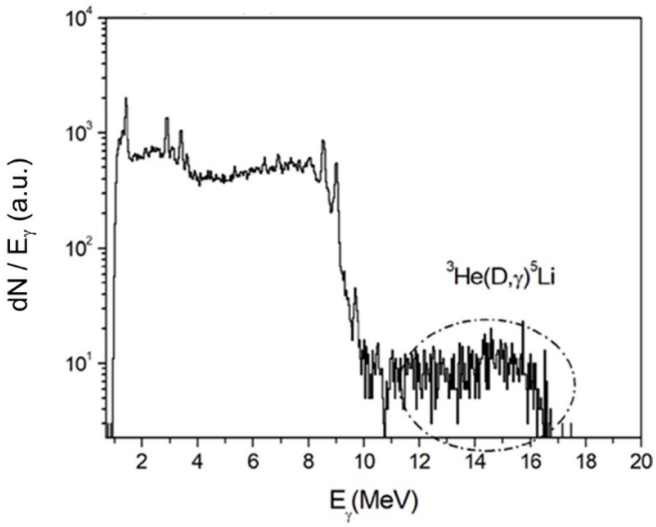

Figure 25. Gamma-ray spectrum (counts per 34 keV) recorded by tangential γ-ray spectrometer in the D-^{3}He plasma discharge #95679; dash-line shows the area related to D(^{3}He,γ)^{5}Li reactions.

For the first time γ-rays from $T(p,\gamma)^4He$ reaction, which realises nuclear energy $Q = 19.8$ MeV were measured in tokamaks. Due to an energetic population of H-ions generated by ICRF in the H-minority heating of the JET T-plasmas, the Doppler broadening of the 20 MeV γ-ray line has been observed. The spectra recorded with vertical and tangential γ-ray spectrometers are presented in figure 24. This reaction can potentially be used for the core temperature measurement in reactor plasmas. Indeed, the γ-ray spectrum of the radiative capture reaction $T(p,\gamma)^4He$ is quite sensitive to the distribution function of D–D fusion protons born in a fusion reactor [55]. An effective electron temperature could be deconvoluted from the line broadening with rather high accuracy since a negligible background is present in this spectrum energy range.

In the JET ^3He-D plasmas, the radiation capture reaction $D(^3He,\gamma)^5Li$ with $Q = 16.4$ MeV is giving rise ≈17 MeV γ-rays. It has been used for fast-ion studies [6] and an example of the energy spectrum recorded with the $LaBr_3$-scintillator detector is represented in figure 25. Furthermore, measurements of 17 MeV γ-rays in ^3He-D plasmas were used for testing of γ-ray diagnostics at a low neutron-induced background in the preparation of the D–T experiments.

Along with the $D(T,n)^4He$ reaction with $Q = 17.59$ MeV, which is distributed between neutron (14.1 MeV) and α-particle (3.5 MeV), the radiation capture reaction $D(T,\gamma)^5He$ with $Q = 16.85$ MeV is a direct indicator of the D–T fusion. Thus, spectrometry of 17 MeV gammas can be a complementary to 14 MeV neutron measurements.

Both radiation capture reactions, $D(T,\gamma)^5He$ and $D(^3He,\gamma)^5Li$, are a factor of $\sim 10^{-5}$ weak branches of the main fusion reactions, however detection of these γ-rays is important as it provides direct information on the fusion α-particle rate and could be used for this purpose in reactors.

Unfortunately, such measurements of the absolute DT-rate values cannot be done with accuracy as good as that of the 14 MeV neutron measurements. The JET fission chambers [56] calibrated with high accuracy [57] provide the D–T fusion rate data with uncertainty less than 10%.

There are several obstacles to do the same with the $D(T,\gamma)^5He$ reaction. The main problem is the uncertainty of the reaction branching ratio [58–61], which is known with accuracy 30%–50%; the second one is the difficulty of a precise quantification of the γ-ray diagnostic response function. Indeed, several factors should be quantified with the required accuracy, including the plasma field of view, neutron and γ-ray attenuation factors. Also, the 17 MeV γ-ray detector response function needs to be precisely characterised. However, it is known that both ground state and the first excited state of the final ^5He-nucleus are rather broad, i.e. the ground state width $\Gamma_{g.s.} \sim 0.6$ MeV; the first excited state width was obtained just from R-matrix model calculations. Furthermore, the response function of the solid-state γ-ray detector consists of continuous γ-ray Compton scattering spectrum, full energy peak and single/double escape peaks. Hence, deconvolution of the detected 17 MeV γ-ray emission is challenging and may be highly uncertain. This becomes obvious from the recorded γ-ray spectrum represented in figure 26.

Nevertheless, the 17 MeV γ-ray rate can be calibrated with the DT-neutron rates provided by the JET fission chambers. Then, this γ-ray data can be used as an additional (or spare) tool for monitoring of the D–T fusion power. Figure 27 shows yields of γ-rays in the energy window 15–17.5 MeV, which were normalised to the D–T neutron yields for several discharges with low tritium concentration that prevents possible uncertainties due to high count-rates. A statistical error of the fitting is less than 10% in spite of the 17 MeV γ-ray rate in these discharges being rather low. So, the errors can be reduced with an optimal diagnostic setup. The example presented in figure 27 demonstrates feasibility of this additional tool for the

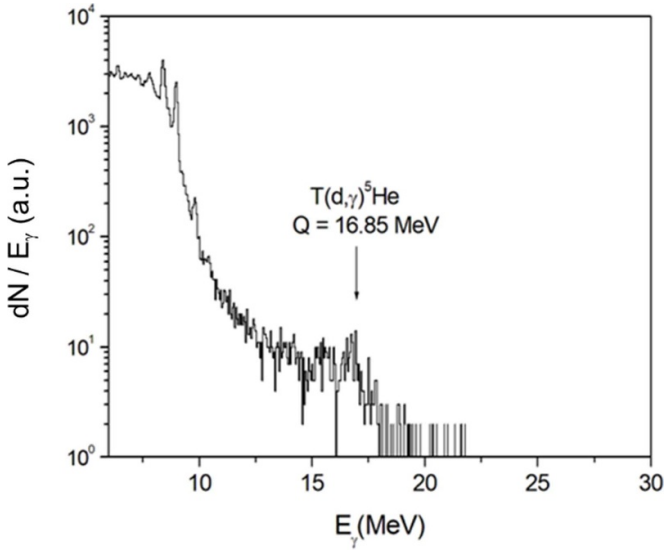

Figure 26. Gamma-ray spectrum (counts per 39 keV) recorded by tangential γ-ray spectrometer in the similar JET D-(T) plasma discharges NBI heating #98043-98 046.

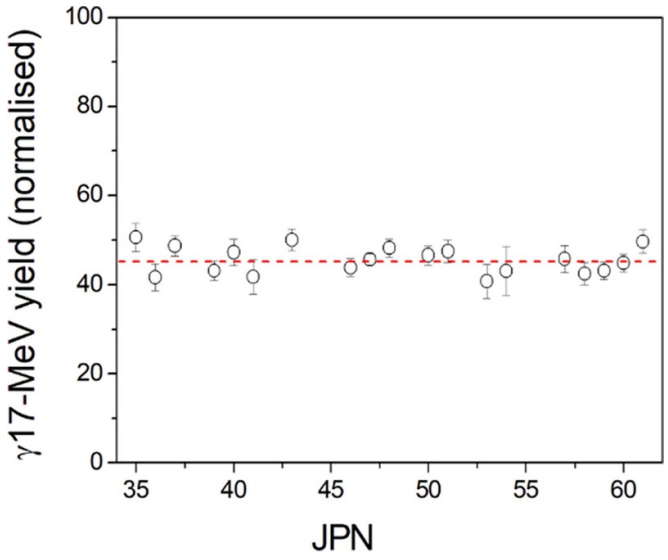

Figure 27. Vertical spectrometer yield of 17 MeV γ-rays (a.u.) normalized to the calibrated D–T neutron yield in discharges with JPN 993xx; dash line shows the fitted average ratio.

D–T fusion rate monitoring with required accuracy. It could be used i.e. in an emergency case when the fission chambers used for the neutron rate measurements have failed.

8. Summary and conclusions

The α-particle confinement is of crucial importance for future reactors. Therefore, the fusion-born α-particle study was a priority task in DTE2, the second JET *D-T* experimental campaign. Selected results of the confined and lost fusion α-particle measurements in these experiments were presented in the paper.

Challenges of the α-particle studies require a significant development of dedicated diagnostics for both confined and lost α-particles. A review of the DTE2 α-particle diagnostics was given. The first-ever results of the confined α-particle diagnosing based on detection of γ-rays of the $^9Be(\alpha,n\gamma)^{12}C$ reaction were shown here.

Direct evidence of the α-particle heating of electrons and assessments of the fusion performance in the special afterglow plasmas were presented. It was found that the afterglow self-heating provides the fusion α-particle power amplification $Q_\alpha \approx 2.2$. Therefore, the study of afterglow plasmas from the point of view of burning plasma physics could be useful in support of the future ITER experiments.

Plasma instabilities may lead to significant α-particle losses. The loss of plasma heating is not acceptable for an efficient fusion plant. Observations of the α-particle loss related to MHD activities in tritium and *D–T* plasmas are presented.

Our first observations of the *T–T* α-particles can also improve knowledge of this fusion reaction that is important for astrophysics as well. In the paper we demonstrated unique results on measurements of 17 MeV γ-rays due to the $D(T,\gamma)^4He$ reaction and 20 MeV γ-rays of the $T(H,\gamma)^4He$ reaction that were measured in the *D-T* plasmas and the tritium plasma with *H*-minority ICRF heating.

Thus, recent JET DTE2 experiments provided unique information on the α-particle behaviour in the ITER relevant scenarios which give opportunity for the further detailed analysis and modelling that could enrich the knowledge on the α-particle physics in fusion reactors with magnetic confinement.

Acknowledgments

This work has been carried out within the framework of the EUROfusion Consortium, funded by the European Union via the Euratom Research and Training Programme (Grant Agreement No 101052200—EUROfusion) and from the RCUK Energy Programme (Grant Number EP/W006839/1). Also, this work partially supported by the U.S. Department of Energy under Contract Number DE-AC02-09CH11466, by the Polish Ministry of Science and Higher Education within the programme 'PMW' for 2022-2023, by the Grants FIS2017-85252-R and PID2021-127727OB-I00, funded by MCIN/AEI/ 10.13039/501100011033 and ERDF 'A way of making Europe'. Views and opinions expressed are however those of the author(s) only and do not necessarily reflect those of the European Union or the European Commission. Neither the European Union nor the European Commission can be held responsible for them. To obtain further information on the data and models underlying this paper please contact PublicationsManager@ukaea.uk.

ORCID iDs

V.G. Kiptily https://orcid.org/0000-0002-6191-7280
R. Dumont https://orcid.org/0000-0002-1030-138X
J. Garcia https://orcid.org/0000-0003-0900-5564
L. Garzotti https://orcid.org/0000-0002-3796-9814

J. Hobirk https://orcid.org/0000-0001-6605-0068
A. Kappatou https://orcid.org/0000-0003-3341-1909
P. Mantica https://orcid.org/0000-0001-5939-5244
S.E. Sharapov https://orcid.org/0000-0001-7006-4876
E.R. Solano https://orcid.org/0000-0002-4815-3407
D. Van Eester https://orcid.org/0000-0002-4284-3992
P.J. Bonofiglo https://orcid.org/0000-0001-5057-7383
T. Craciunescu https://orcid.org/0000-0002-0012-4260
A. Dal Molin https://orcid.org/0000-0003-0471-1718
J. Eriksson https://orcid.org/0000-0002-0892-3358
M. Nocente https://orcid.org/0000-0003-0170-5275
M. Podestà https://orcid.org/0000-0003-4975-0585
M. Poradzinski https://orcid.org/0000-0002-1858-4046
D. Rigamonti https://orcid.org/0000-0003-0183-0965
J. Rivero-Rodriguez https://orcid.org/0000-0001-5074-0267
Z. Stancar https://orcid.org/0000-0002-9608-280X
H. Sun https://orcid.org/0000-0003-0880-0013
D.M. Taylor https://orcid.org/0000-0002-0465-2466
M. Garcia-Munoz https://orcid.org/0000-0002-3241-502X
C.F. Maggi https://orcid.org/0000-0001-7208-2613
M. Maslov https://orcid.org/0000-0001-8392-4644
C. Perez Von Thun https://orcid.org/0000-0002-1166-2179

References

[1] Maggi C.F. *et al* 2024 Overview of T and D-T results in JET with ITER-like wall *Nucl. Fusion Special Issue: Overview and Summary Papers from the 29th Fusion Energy Conf. (London, UK, 16–21 October 2023)* submitted (https://doi.org/10.1088/1741-4326/ad3e16)
[2] Kiptily V.G. *et al* 2023 *Phys. Rev. Lett.* **131** 075101
[3] Strachan J.D. *et al* 1997 *Plasma Phys. Control. Fusion* **39** B103
[4] Keilhacker M. *et al* 1999 *Nucl. Fusion* **39** 209
[5] Zastrow K.-D. *et al* 2004 *Plasma Phys. Control. Fusion* **46** B255
[6] Kiptily V.G. *et al* 2022 *Plasma Phys. Control. Fusion* **64** 064001
[7] Adams J.M., Jarvis O.N., Sadler G.J., Syme D.B. and Watkins N. 1993 *Nucl. Instrum. Methods Phys. Res.* **A329** 277
[8] Jarvis O.N. 1997 *Plasma Phys. Control. Fusion* **39** 1571
[9] Kiptily V.G. *et al* 2005 *Nucl. Fusion* **45** L21
[10] Nocente M. *et al* 2020 *Plasma Phys. Control. Fusion* **62** 014015
[11] Kiptily V.G., Cecil F.E. and Medley S.S. 2006 *Plasma Phys. Control. Fusion* **48** R59
[12] Curuia M. *et al* 2017 *Fusion Eng. Des.* **123** 749
[13] Nocente M. *et al* 2021 *Rev. Sci. Instrum.* **92** 043537
[14] Nocente M. *et al* 2010 *Rev. Sci. Instrum.* **81** 10D321
[15] Kiptily V.G. *et al* 1990 *Fusion Technol.* **18** 583
[16] Kiptily V.G. *et al* 2002 *Nucl. Fusion* **42** 999
[17] Mantsinen M.J. *et al* 2002 *Phys. Rev. Lett.* **88** 105002
[18] Kiptily V.G., Baranov Y.F., Barnsley R., Bertalot L., Hawkes N.C., Murari A., Popovichev S., Sharapov S.E., Stork D. and Yavorskij V. 2004 *Phys. Rev. Lett.* **93** 1150012
[19] Kiptily V.G. *et al* 2010 *Nucl. Fusion* **50** 084001
[20] Nocente M. *et al* 2012 *Nucl. Fusion* **52** 063009
[21] Tardocchi M. *et al* 2011 *Phys. Rev. Lett.* **107** 205002
[22] Darrow D.S., Bäumel S., Cecil F.E., Kiptily V., Ellis R., Pedrick L. and Werner A. 2004 *Rev. Sci. Instrum.* **75** 3566
[23] Bonofiglo P.J., Kiptily V., Horton A., Beaumont P., Ellis R., Cecil F.E. and Podesta M. 2020 *Rev. Sci. Instrum.* **91** 093502
[24] Baumel S. *et al* 2004 *Rev. Sci. Instrum.* **75** 3563
[25] Rivero-Rodriguez J.F. *et al* 2021 *Rev. Sci. Instrum.* **92** 043553
[26] Kiptily V.G. *et al* 2018 *Nucl. Fusion* **58** 014003
[27] Hawryluk R.J. *et al* 1994 *Phys. Rev. Lett.* **72** 3533 (available at: https://journals.aps.org/prl/pdf/10.1103/PhysRevLett.72.3530)
[28] Taylor G., Strachan J.D., Budny R.V. and Ernst D.R. 1996 *Phys. Rev. Lett.* **76** 2722
[29] Thomas P.R. *et al* 1998 *Phys. Rev. Lett.* **80** 5548
[30] Hobirk J. *et al* 2023 *Nucl. Fusion* **63** 112001
[31] Dumont R.J. *et al* 2018 *Nucl. Fusion* **58** 082005
[32] Stix T.H. 1972 *Plasma Phys.* **14** 367
[33] Spitzer L. Jr 1962 *Physics of Fully Ionized Gases* (Interscience)
[34] Breslau J., Gorelenkova M., Poli F., Sachdev J., Pankin A., Perumpilly G., Xingqiu Y. and Glant L. and USDOE Office of Science TRANSP *Computer software. USDOE Office of Science (SC), Fusion Energy Sciences (FES)* (Accessed 27 June 2018) (https://doi.org/10.11578/dc.20180627.4)
[35] Štancar Ž. *et al* 2023 *Nucl. Fusion* **63** 126058
[36] MCNP® Website (lanl.gov) (available at: https://mcnp.lanl.gov/index.html)
[37] Schoepf K., Yavorskij V., Goloborod'ko V. and Reznik S. 2002 *Kerntechnik* **67** 285
[38] Yavorskij V., Goloborod'ko V., Eriksson L.-G., Kiptily V., Schoepf K. and Sharapov S.E. 2015 *J. Fusion Energy* **34** 774–84
[39] Gatu Johnson M. *et al* 2008 *Nucl. Instrum. Methods Phys. Res.* A **591** 417–30
[40] Fitzgerald M. *et al* 2023 *Nucl. Fusion* **63** 112006
[41] Bonofiglo P.J. *et al* 2024 Alpha particle loss measurements and analysis in JET DT plasmas *Nucl. Fusion* submitted
[42] von Thun C.P. *et al* 2012 *Nucl. Fusion* **52** 094010
[43] Fitzgerald M. *et al* 2019 *Nucl. Fusion* **59** 016004
[44] Coppi B. and Porcelli F. 1988 *Fusion Technol.* **13** 447
[45] Garzotti L. *et al* 2023 Development of baseline scenario for high fusion performance at JET *Nucl. Fusion* submitted
[46] Sharapov S.E. *et al* 2023 *Nucl. Fusion* **63** 112007
[47] Kazakov Y., Ongena J., Van Eester D., Bilato R., Dumont R., Lerche E., Mantsinen M. and Messiaen A. 2015 *Phys. Plasmas* **22** 082511
[48] Kiptily V.G. *et al* 2009 *Nucl. Fusion* **49** 065030
[49] Baranov Y., Jenkins I., Kiptily V., Ongena J. and Yavorskij V. 2010 EuroPhysics Conference Abstracts *37th EPS Conf. On Plasma Physics* vol 34A (*Dublin*) p P5.141 (available at: https://info.fusion.ciemat.es/OCS/EPS2010PAP/pdf/P5.141.pdf)
[50] Kirov K.K. *et al* 2023 Analysis of fusion alphas interaction with RF waves in D-T plasma at JET *Nucl. Fusion* **64** 086011
[51] Jarmie N. and Allen R.C. 1958 *Phys. Rev.* **111** 1121
[52] Allen K.W., Almqvist E., Dewan J.T., Pepper T.P. and Sanders J.H. 1951 *Phys. Rev.* **82** 262 (available at: https://journals.aps.org/pr/pdf/10.1103/PhysRev.82.262)
[53] Wong C., Anderson J.D. and McClure J.W. 1965 *Nucl. Phys.* **71** 106

[54] Database ENDF TENDL-19 (available at: www.oecd-nea.org)
[55] Kiptily V.G. *et al* 2015 *Nucl. Fusion* **55** 023008
[56] Jarvis O.N. 1994 *Plasma Phys. Control. Fusion* **36** 209
[57] Batistoni P. *et al* 2018 *Nucl. Fusion* **58** 106016
[58] Morgan G.L. *et al* 1986 *Phys. Rev.* **C33** 1224 (available at: https://journals.aps.org/prc/pdf/10.1103/PhysRevC.33.1224)
[59] Cecil F.E. and Wilkinson F.J. 1984 *Phys. Rev. Lett.* **53** 767 (available at: https://journals.aps.org/prl/pdf/10.1103/PhysRevLett.53.767)
[60] Kim Y. *et al* 2012 *Phys. Plasmas* **19** 056313
[61] Dal Molin A. *et al* 2024 Measurement of the gamma ray to neutron branching ratio for the deuterium-tritium reaction in magnetic confinement fusion plasmas *Phys. Rev. Lett.* submitted